

REPORT DOCUMENTATION PAGE

Form Approved
OMB NO. 0704-0188

Public Reporting burden for this collection of information is estimated to average 1 hour per response, including the time for reviewing instructions, searching existing data sources, gathering and maintaining the data needed, and completing and reviewing the collection of information. Send comment regarding this burden estimates or any other aspect of this collection of information, including suggestions for reducing this burden, to Washington Headquarters Services, Directorate for Information Operations and Reports, 1215 Jefferson Davis Highway, Suite 1204, Arlington, VA 22202-4302, and to the Office of Management and Budget, Paperwork Reduction Project (0704-0188,) Washington, DC 20503.

1. AGENCY USE ONLY (Leave Blank)		2. REPORT DATE January 29, 2006		3. REPORT TYPE AND DATES COVERED Final Progress Report - July 01, 2002 - June 30, 2005	
4. TITLE AND SUBTITLE TEES Final Progress Report to ARO on the project, "Magnetic Shape Memory Alloys with High Actuation Forces"				5. FUNDING NUMBERS DAAD 19-02-1-0261	
6. AUTHOR(S) Ibrahim Karaman and Dimitris C. Lagoudas					
7. PERFORMING ORGANIZATION NAME(S) AND ADDRESS(ES) Texas Engineering Experiment Station (TEES), 334 WERC Bldg., MS 3000 College Station, Texas 77843-3000				8. PERFORMING ORGANIZATION REPORT NUMBER ARO-TEES68210-FPR	
9. SPONSORING / MONITORING AGENCY NAME(S) AND ADDRESS(ES) U. S. Army Research Office P.O. Box 12211 Research Triangle Park, NC 27709-2211				10. SPONSORING / MONITORING AGENCY REPORT NUMBER 43794.4-MS	
11. SUPPLEMENTARY NOTES The views, opinions and/or findings contained in this report are those of the author(s) and should not be construed as an official Department of the Army position, policy or decision, unless so designated by other documentation.					
12 a. DISTRIBUTION / AVAILABILITY STATEMENT Approved for public release; distribution unlimited.				12 b. DISTRIBUTION CODE	
13. ABSTRACT (Maximum 200 words) The specific aims of the project are: 1) Understand governing mechanisms and important physical, mechanical and magnetic parameters responsible for magnetic shape memory phenomena in MSMA alloys in single crystalline form, 2) to develop new nickel, iron or cobalt base ferromagnetic alloy compositions to increase attainable actuation stress levels and to reveal new mageto-thermo-mechanical mechanisms, 3) to conduct experiments to evaluate whether these compositions will result in good magnetic shape memory response and high actuation force, and 4) to develop a thermodynamically sound model that will predict the coupled effects of mechanical load, magnetic field and temperature on magnetic shape memory behavior. The main accomplishments in the project are: 1) the maximum actuation stress level was increased from 2 MPa to 5 MPa for the magnetic field induced martensite reorientation mechanism for the same amount of actuation strain (6%). 2) For the first time, the team observed cyclic magnetic field induced martensite to austenite transformation. This was confirmed using in-situ magnetic field experiments in an XRD at Argonne National Lab. 3) By utilizing this new actuation mechanism, the team was able to increase the cyclic actuation stress to 24 MPa with about 0.5% actuation strain. These numbers can be increased further. The mechanism has also resulted in field-induced one-way shape memory effect. In this effect, the actuation stress varied between 60 to 100 MPa with actuation strain levels are up to 3%. 4) The team found out the conditions to obtain magnetoelasticity utilizing the above two microstructural mechanisms under cycling loading (cyclic stress under magnetic field or magnetic field under constant stress). 5) development of a thermodynamically consistent phenomenological model which captures the ferromagnetic shape memory effect, i.e. the large macroscopically observable shape change of magnetic shape memory materials under the application of external magnetic fields and magnetization evolution. The significance of these accomplishments is that the selected compositions after specific thermomechanical treatments are revealed promising new actuation mechanism and increased the actuation stress and work output levels an order of magnitude. For further details, see the attached technical report.					
14. SUBJECT TERMS Magnetic shape memory alloys, martensitic phase transformation, thermoelastic martensite				15. NUMBER OF PAGES	
				16. PRICE CODE	
17. SECURITY CLASSIFICATION OR REPORT UNCLASSIFIED	18. SECURITY CLASSIFICATION ON THIS PAGE UNCLASSIFIED	19. SECURITY CLASSIFICATION OF ABSTRACT UNCLASSIFIED	20. LIMITATION OF ABSTRACT UL		

NSN 7540-01-280-5500

Standard Form 298 (Rev.2-89)
Prescribed by ANSI Std. Z39-18
298-102

TABLE of CONTENTS

	<u>Page</u>
Memorandum of Transmittal	1
Report of Inventions and Subcontractors	2
Table of Contents	3
1. Statement of the problem studied	4
2. Summary of Important Results	7
2.1. Modeling work	40
2.1.1. Derivation of the Model	40
2.1.2. A numerical example of the application of the model	43
3. Listing of all publications and technical reports supported under this grant or contract	48
4. List of all Participating Scientific Personnel showing any Advanced Degrees Earned by them while employed on the Project	50
Report of Inventions	51
Bibliography	51
Appendixes	53
Report Documentation Page	54

TEES Final Report to ARO on the project: Magnetic Shape Memory Alloys with High Actuation Force

January 29, 2006

by I. Karaman and D.C. Lagoudas

1. Statement of the problem studied

Magnetic Shape Memory Alloys (MSMAs) have attracted an increasing interest in the past few years due to their unique actuation, sensing and power generation capabilities [1-13]. Conventional actuator materials such as piezoelectric and magnetostrictive materials have the advantage of fast response and high actuation stress levels [14-15] but yield only small strains. Magnetostrictive Terfenol-D ($Tb_{0.27}Dy_{0.73}Fe_2$) gives a strain of less than 0.2% and maximum actuation stress level of about 60 MPa in a magnetic field of about 0.2 – 0.3 Tesla [16], but rare earth metals are expensive [14]. PZT (lead-zirconate-titanate) piezoceramics result in a maximum strain of about 0.1% and maximum actuation stress level of about 100 MPa [17] in an electric field of several hundred V/cm [15]. However, PZT is an oxide and thus brittle. By contrast, conventional shape memory alloys (SMAs) can yield high actuation stresses (few hundred MPas) and strains on the order of 8%, but show slow response due to the restriction of heat transfer [18]. The recently developed MSMAs offer the possibility of both large actuation strains, comparable to those of conventional SMAs and response frequencies in the kHz regime [19]. However, the currently available actuation stress levels are very low (a few MPas) [6].

There are two possible mechanisms for obtaining large magnetic field induced strains (MFIS) in MSMAs. The first one, which has been studied extensively since 1996 [2], involves the field-induced reorientation of microstructural variants (martensite twins). In this mechanism, the magnetic field triggers the motion of martensite twin interfaces such that twins with favorably oriented magnetization axis grow at the expense of other twins leading to an external shape change (Figure 1.a). The mechanism requires simultaneous application of external stress and magnetic field to obtain reversible shape change. The field-induced martensite twin reorientation is possible in materials with high magnetocrystalline anisotropy energy (MAE) and low energy of twin boundary motion. The intermetallic Ni_2MnGa and $FePd$ alloys are the most widely explored MSMAs [1-10, 20-21] since only these have been reported to demonstrate MFIS of more than 1% via the aforementioned mechanism.

The main limiting factor in currently available MSMAs which solely use the above mechanism is low actuation stress levels of usually less than 3 MPa [3-6, 9-10]. Moreover, the operating temperature range is quite narrow [11-12] as the upper temperature limit is martensite to parent phase transformation temperature (A_s) and the lower limit is a critical temperature where the energy required for twin boundary motion exceeds the MAE. For many applications, it is important to increase the operating temperature interval and actuation stress levels from a few MPas to the order of hundred MPa.

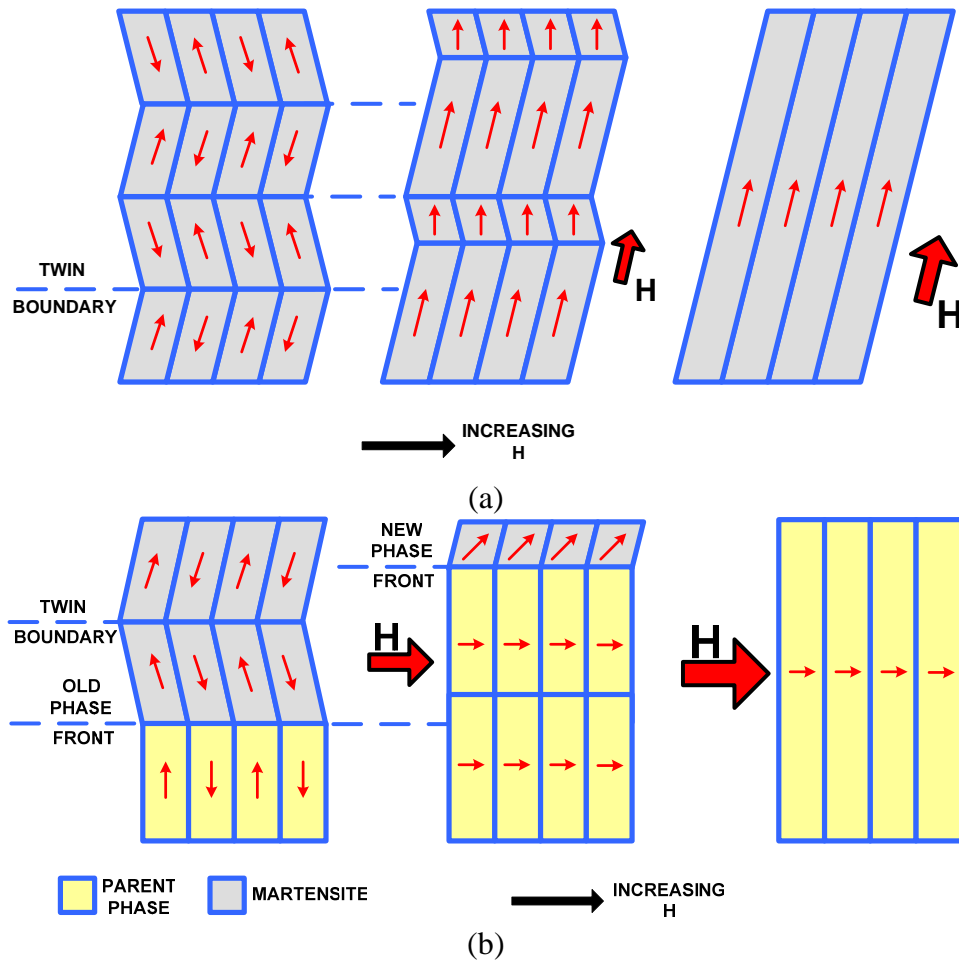


Figure 1. Effect of applied magnetic field, H , on the reorientation of the martensite twin variants (a), and phase transformation (b) in MSMA.

The second possible mechanism to induce large MFIS is the magnetic field-induced phase transformation (Figure 1.b). The field-induced martensitic phase transformation has been detected in several ferromagnetic materials such as Fe-C and Fe-Ni in the past [22-25], under very high field magnitudes (>15 Tesla) without any report of observed MFIS levels. Certain Fe-Ni-Co-Ti alloys demonstrated reversible martensitic transformation but only under the application of a high pulsed magnetic field (~ 30 Tesla) [22]. Obviously, the need for giant magnetic fields severely limits the use in actual applications. The possibility to induce a reversible phase transformation with low magnetic field magnitudes has not been explored in detail in MSMA.

The goal of this project was to understand the mechanisms responsible for magnetic shape memory effect and parameters that determine the actuation stress levels in MSMA, and develop new materials and microstructures to increase the currently attainable actuation stress levels. In addition, to reveal the coupled effects of physical, mechanical, and magnetic parameters which are otherwise difficult to do with experimentation, the development of thermodynamically sound constitutive modeling of MSMA behavior model that would consider loading history dependence of the state variables or hysteresis effects was planned. Following these goals, the team has focused on the following major research tasks:

1. Understand governing mechanisms and important physical, mechanical and magnetic parameters responsible for magnetic shape memory phenomena via field-induced martensite reorientation in existing MSMA single crystals (NiMnGa alloys) through a well-structured experimental plan. Develop a state-of-the-art magneto-thermo-mechanical testing set-up to conduct experiments.
2. Develop new material compositions in NiMnGa alloy system to utilize field-induced phase transformation in MSMA for possible increase of actuation stress level. Determine the materials parameters and governing mechanisms responsible for field-induced phase transformation in single crystals.
3. Develop new alloy compositions from Co and Fe based alloys that would demonstrate magnetic shape memory effect and result in higher actuation stress levels than Ni based alloys. Fabricate textured polycrystalline materials from selected Fe based compositions using powder consolidation under magnetic field via Equal channel angular extrusion. Equal channel angular extrusion (ECAE) is a potential powder consolidation method that overcomes some of the difficulties associated with HIPing and conventional extrusion. The ECAE technique involves subjecting the powder to high pressure and simple shear in a die containing intersecting channels [26-28]. Potential benefits of the ECAE process are: constant workpiece cross-section, uniform deformation throughout workpiece and consolidation to near full density after a single extrusion [29].
4. Develop a thermodynamically sound model that will consider loading history dependence of the state variables or hysteresis effects that cannot be accounted for with current energy minimization approaches. Validate the model with currently available experimental results and with the results that will be obtained in the present work. Predict the coupling effects of temperature, mechanical force, and magnetic field on martensite reorientation, transformation and recoverable strains. These predictions will be helpful in determining the processing parameters and the conditions to obtain maximum magnetic shape memory strain.

The proposed investigations have achieved the following key accomplishments:

- ◆ Developed a magneto-thermo-mechanical test set-up. The set up has following features: 1) bipolar magnetic fields up to 3 Tesla, 2) cyclic temperature range of -190 °C to 225 °C, 3) simultaneous control of stress/strain, temperature and magnetic field rates, 4) precise measurement of strain, stress and temperature in the magnetic field, 5) in-situ magnetization measurement as a function of stress, magnetic field and temperature.
- ◆ Through a detailed characterization work on a NiMnGa alloy single crystals, identified physical parameters that would determine the actuation strain and stress. Some of these parameters are saturation magnetization, magnetocrystalline anisotropy energy, twin boundary mobility, martensitic transformation temperatures and Curie temperatures. By modifying some of these parameters and composition, we have achieved the following:

- 1) The maximum actuation stress reported to date was less than 2 MPa. This stress level was increased to 5 MPa for the magnetic field induced martensite reorientation mechanism for the same amount of actuation strain (6%).
 - 2) For the first time, the team observed cyclic magnetic field induced martensite to austenite transformation. This was confirmed using in-situ magnetic field experiments in an XRD at Argonne National Lab.
 - 3) By utilizing this new actuation mechanism, the team was able to **increase the cyclic actuation stress to 24 MPa** with about 0.5% actuation strain. These numbers can be increased further. The mechanism has also resulted in field-induced one-way shape memory effect. In this effect, the actuation stress varied between 60 to 100 MPa with actuation strain levels are up to 3%.
 - 4) The team found out the conditions to obtain magnetoelasticity utilizing the above two microstructural mechanisms under cycling loading (cyclic stress under magnetic field or magnetic field under constant stress).
- ◆ Identified new materials and compositions (total of 4) to increase the actuation stress further by using the criteria that we came up with. The purpose in the first three (FeNiGa, CoNiGa and CoNiAl) is to increase the actuation stress during magnetic field induced martensite reorientation and martensite to austenite transformation. The idea for the last composition (a CoNiAl alloy) is to study the magnetic field induced phase transformation. From preliminary experiments, the actuation strain will be somewhere in between 4 to 10%. With this strain level and actuation stress, the actuation energy density will be significantly larger as compared to NiMnGa. Moreover, the new materials significantly more ductile which is important for formability. However, there was not sufficient time to characterize these new materials in detail for their coupled magneto-thermo-mechanical behavior.
 - ◆ Successful growth of single crystals in several different Fe, Co and Ni based ferromagnetic alloys. It should be noted that the single crystal growth from these alloys is not trivial since the chemical inhomogeneity may cause problems at times.
 - ◆ Developed a microstructural mechanism based continuum level coupled constitutive models considering the effects of magnetic field, stress and temperature, history dependence and length scales. With this model, it is possible to accurately capture magnetic field induced strain and magnetization evolution as a function of stress and magnetic field. Accurate magnetization evolution prediction simultaneously with stress-field-strain behavior predictions is phenomenal.

Improvements in material systems, and an understanding of the magneto-thermo-mechanical behavior of those systems for the actuator applications, will have a positive influence and impact on other potential applications of magnetic shape memory alloys.

2. Summary of Important Results

During the period of July, 2002 to June, 2005 the following notable results were achieved. First two list the most important findings that have implications for our continuing research and others give more detailed information on what has been done in the present project:

1. Magnetic shape memory properties of a single crystal Ni₂MnGa alloy were characterized through monitoring magnetic field induced strain (MFIS) as a function of compressive stress,

and applied stress induced strain as a function of magnetic field. Compressive stress and magnetic field were applied perpendicular to each other along the [100] and [011] axes, respectively. It was revealed that increasing constant magnetic field level significantly increases the stress required for the reorientation, i.e. magnetostress and leads to superelasticity in martensite. Moreover, it was observed that the MFIS evolution is field rate dependent as was evidenced by a rate dependent two-stage reorientation where the maximum MFIS magnitude increases as the field rate increases. This effect was attributed to the difference between the nucleation and propagation barrier strength for twin boundary motion in NiMnGa alloys. ***The magnetostress (5.7 MPa), blocking stress (5 MPa) and maximum MFIS (5.8%) combination observed in this study is the highest reported to date in NiMnGa alloys*** (details of these results will be explained below). The high blocking and magnetostresses are a consequence of the low test temperature (-95 °C) where the magnetocrystalline anisotropy energy is high and detwinning stress is low. Thus, for magnetic shape memory alloys, the selection of the operating temperature with respect to martensite start and Curie temperatures is critical in optimizing actuator performance since both magnetocrystalline anisotropy energy and detwinning stress are a strong function of temperature below the characteristic temperatures.

- 2. Magnetic field-induced phase transformation under low field magnitudes was demonstrated as a new mechanism for at least an order of magnitude increase in actuation stress and work output levels in NiMnGa magnetic shape memory alloys*** (MSMAs). First, the effect of magnetic field on the martensitic phase transformation in off-stoichiometric Ni₂MnGa MSMA single crystals was investigated with a simultaneous application of compressive stress. A two-stage stress-induced martensitic phase transformation was observed in which the magnetic field increased the transformation stress levels. In the first stage, which was characterized as the parent to orthorhombic martensite phase transformation, the magnetic field led to the separation of pseudoelastic loops with and without the field. A maximum reversible magnetic-field induced strain (MFIS) of 0.5% was observed under 24 MPa compressive stress in the first stage phase transformation at -60 °C. In the second stage, which was the transformation from the orthorhombic martensite phase to 5M martensite, one-way MFISs of up to 4% were achieved under different stress magnitudes as high as 110 MPa depending on the operating temperature (more details about these results can be found below). The work output levels achieved in the first-stage transformation were comparable to the work outputs attained using the field-induced martensite reorientation in NiMnGa MSMAs, however, the actuation stress levels were an order of magnitude higher. In the second stage, it was possible to achieve one order of magnitude higher work outputs than the former two cases. The present work output levels achieved in the Ni₂MnGa MSMA and the outlook for the further increase place MSMAs significantly above many currently available high frequency active materials such as ferroelectrics and magnetostrictive materials in terms of work output.

To compare the actuation performance of all published NiMnGa alloy compositions with the present results, we considered the field-induced mechanical work output (work per unit volume) under constant stress (= MFIS x actuation stress) as a figure of merit and constructed Figure 2 in logarithmic scale.

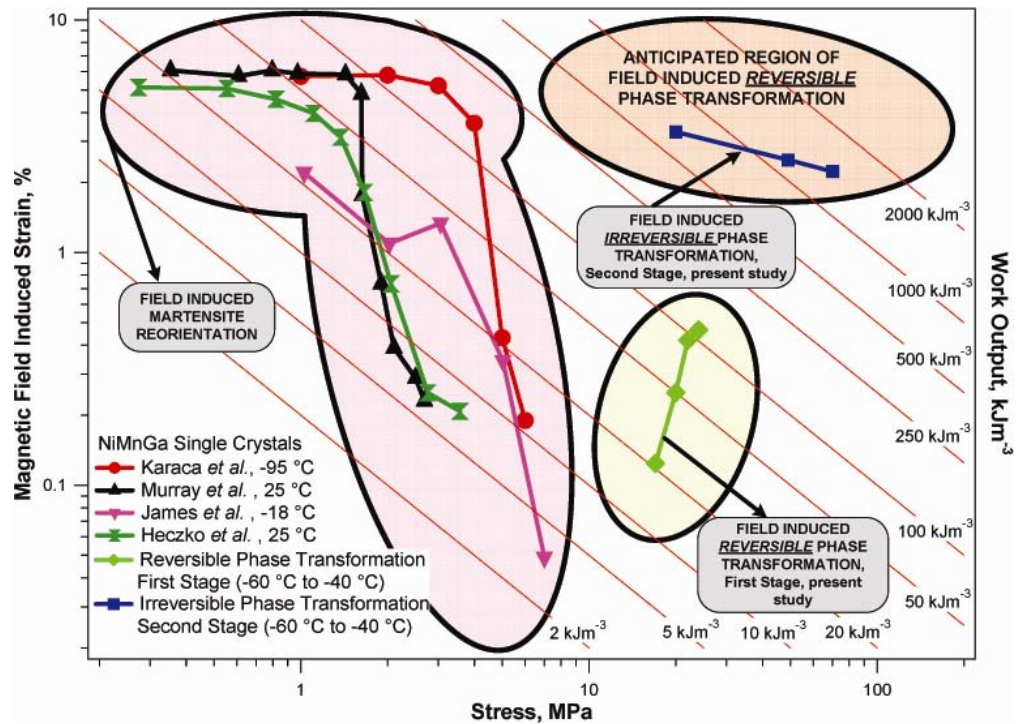


Figure 2. MFIS and work output vs. the actuation stress plots showing the literature data obtained to date utilizing field-induced martensite reorientation mechanism and the present results of field-induced martensite reorientation and field-induced reversible and irreversible phase transformations in NiMnGa MSMAs. The figure also shows a region of MFIS, actuation stress and work output that might possibly be achieved utilizing the simple guidelines introduced here and optimizing the suggested parameters. A grid of constant mechanical work output hyperbolas ranging from 2 and 2000 kJm⁻³ has been superimposed. Logarithmic scale is used for both axes for easy comparison.

The figure is divided into three regions. The left hand side of the figure (the first region) consists of the previously published MFIS, actuation stress and work output levels due to field-induced martensitic variant reorientation and the present results utilizing this mechanism [6, 9-10, 13]. The lower right hand corner (the second region) demonstrates the present results for the reversible field-induced phase transformation in the first transformation stage. In this region, a maximum cyclic MFIS of 0.5% under 24 MPa was obtained. The work output in this region is similar to that from the field-induced variant reorientation (the first region), however, the actuation stress is almost one order of magnitude higher in the former. The solid line on the upper right hand corner (the third region) shows the actuation stress, MFIS, and work output levels from the irreversible field-induced phase transformation (one-way shape memory effect) in the second transformation stage of the present alloy. In this response, the work output increases from 660 to 1600 kJm⁻³ as the temperature increases from -80 to -40 °C demonstrating that it is possible to achieve over more than one order of magnitude higher work output and actuation stress as compared to that of field-induced variant reorientation. The third region also includes the area of anticipated performance levels that can possibly be achieved in NiMnGa alloys and other ferromagnetic SMAs. This simply requires identification of alloy compositions and phase structures in which magnetic field application would separate the pseudoelastic stress

hysteresis loops with and without field. *Note that the work output levels achieved in the second and third regions are considerably higher than the work outputs from other active materials such as piezoelectrics and magnetostrictive materials* [14, 30].

3. Selection and successful single crystal growth in Ni_2MnGa , $\text{Ni}_{50}\text{Mn}_{30}\text{Ga}_{20}$, $\text{Co}_{38}\text{Ni}_{33}\text{Al}_{29}$, $\text{Co}_{49}\text{Ni}_{21}\text{Ga}_{30}$, $\text{Co}_{35}\text{Ni}_{35}\text{Al}_{30}$, Fe-29Ni-22Co-4Ti, and Fe-35Co-19Ni-9Ti alloys. They were acquired from DOE Ames Laboratory, Special Metals Corporation and Sophisticated Alloys in cast form. *Some of the cobalt and iron based alloys are new and we are the first group who studied conventional and magnetic shape memory effect in these materials.*
4. *We have built a magneto-thermo-mechanical (MTM) test set-up.* A schematic of this setup is shown in Figure 3 and the experiments that we have conducted using this set up is summarized in Table 1 with respect to the control parameters. *This set-up is one of a kind because of its temperature range and simultaneous control of stress, magnetic field and temperature while also measuring strain and magnetization.* The details of the test set up are explained shortly above and in the previous annual reports. Figure 4 shows representative digital images of the MTM test set-up. The overall set-up let us investigate the effect of coupled magnetic, mechanical and thermal fields under monotonic and cyclic loading conditions as we can cycle load, magnetic field and temperature. Figure 5 shows an example of the recorded stress, strain, magnetic field and temperature data during an experiment under a constant stress of 3 MPa at $-95\text{ }^\circ\text{C}$. The results mentioned in items 1 and 2 were achieved using this test set-up.

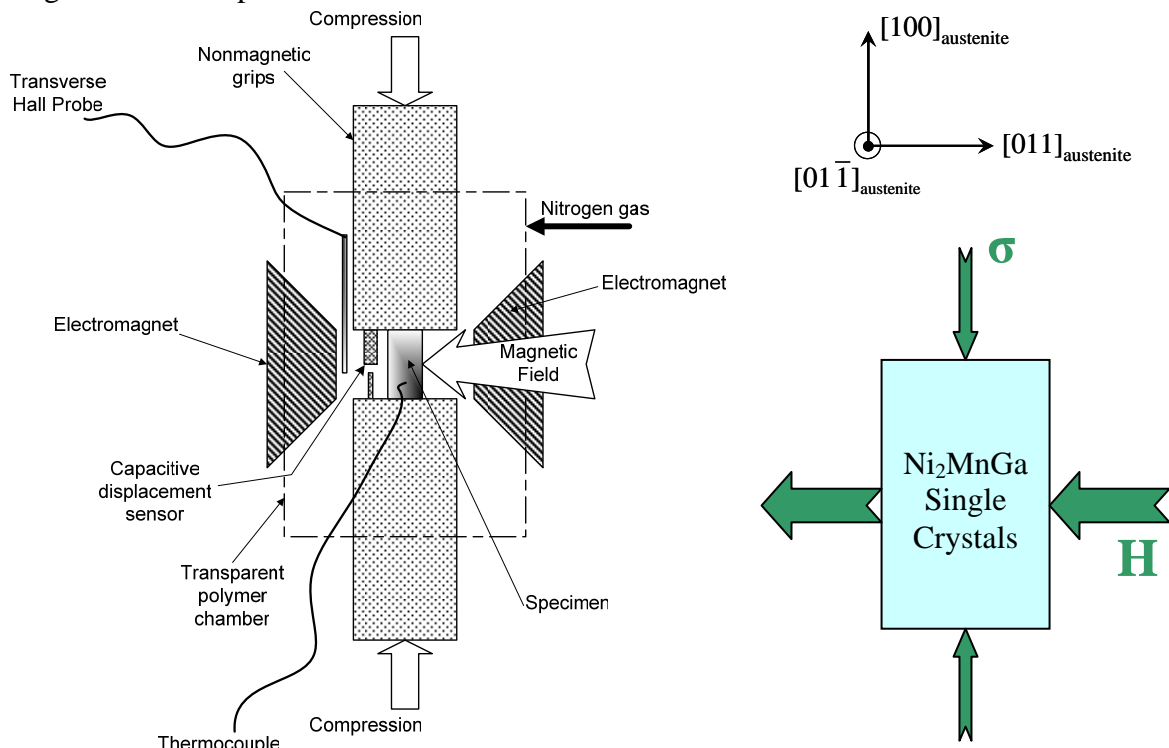


Figure 3. Schematic of the magneto-thermo-mechanical setup with an electromagnet and a capacitive displacement sensor developed in this project.

Table 1: Summary of the experiments conducted and the parameters that are either controlled or measured using the magneto-thermo-mechanical testing set-up. The resulting behavior is also given in the table. These experiments are initially conducted on Ni₂MnGa single crystals.

Temp	σ	H	ϵ	T	done	Comments
$\langle M_f \rangle$ or $\langle A_s \rangle$	Fixed	Variable	Measured	Fixed	Y	Butterfly curves
$\langle M_f \rangle$ or $\langle A_s \rangle$	Variable	Fixed	Measured	Fixed	Y	Magnetoelastic response
$\langle M_f \rangle$ or $\langle A_s \rangle$	Fixed	Variable rate	Measured	Fixed	Y	Magnetic Field rate effect
$\langle A_f \rangle$	Variable	Fixed	Measured	Fixed	Y	Effect of H on PE curves
Additional variable: orientation.						

5. Using the above set up and experimental conditions presented in Table 1, the magneto-mechanical response of the Ni₂MnGa single crystals oriented along the [100] direction was investigated considering the effect of field cycles, temperature and field rate on the magnetic field induced strain, blocking stress and magnetostress, magnetoelasticity and magnetoplasticity. The magnetic field and external stress were applied perpendicular to each other at -95 °C. The main results of this study can be summarized as follows (more details can be found in Reference 6):

- i. *The maximum magnetic field induced field strain (MFIS) levels are found to be a function of applied stress* (Figures 6 and 7). Increasing stress decreases the MFIS and no MFIS is observed above the blocking stress (Figure 8). Figures 6.a and 6.b show the effect of magnetic field on strain under constant compressive stress and temperature for increasing and decreasing stress levels from 2 MPa to 6 MPa and 5 MPa to 1 MPa, respectively. Before each test, the stress of 6 MPa was applied and unloaded to the desired stress level in order to obtain the same single variant martensite morphology. A total of three magnetic field cycles were applied between 16 kG and -16 kG. To better understand the cycle effect, the first and second cycle responses are plotted separately in Figure 7.a and 7.b, respectively. Although the maximum MFIS decreases with stress level for the first cycle, it surprisingly increases first and then decreases in the second cycle (Figure 8). Moreover, the maximum MFIS for the first cycle is always greater than the

one for the second cycle. **The blocking stress is about 5 MPa.** The irrecoverable MFIS which is the MFIS difference between the first and second cycles decreases with stress level and vanishes completely for the stress levels of 5 MPa and higher. These are attributed to the competition between the stress and magnetic field favored martensite variants during the forward and backward reorientation (Figure 9). It is also clear in Figure 7.b that the critical magnetic field needed for martensite reorientation increases with stress magnitude. **The maximum MFIS is 5.8% which is close to the theoretical maximum reorientation strain for the 5M tetragonal martensite.**

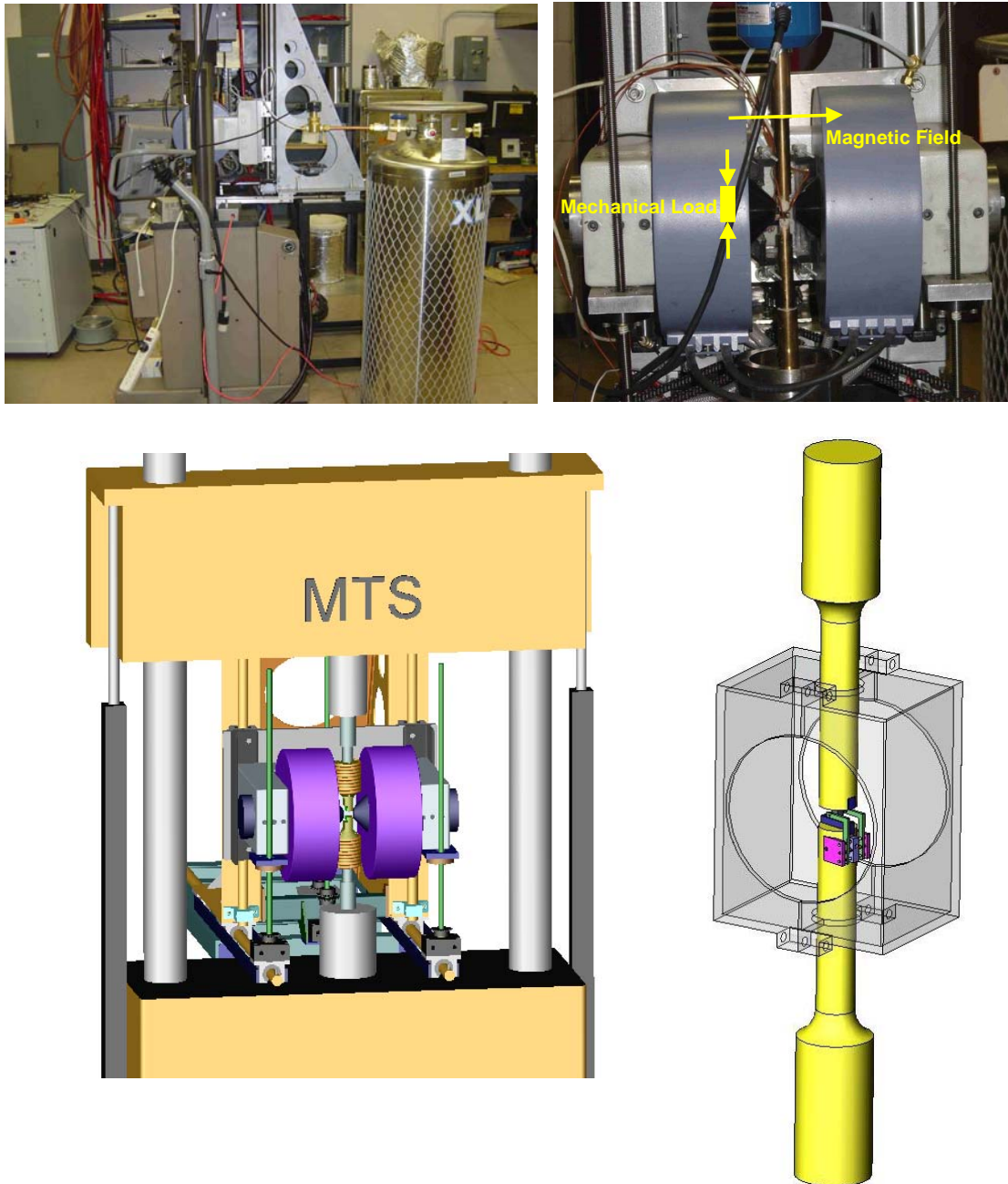


Figure 4. Digital images and schematic of the details of the magneto-thermo-mechanical test set up that has been built in this project.

ii. The magnetic field rate has a significant effect on the MFIS evolution (Figures 10 and 11). At lower field rates (< 150 kG/sec), *a rate dependent two stage reorientation is observed where the maximum MFIS magnitude increases with the field rate* (Figure 12). This was attributed to the difference between the nucleation and propagation barrier strength for twins. In Figure 11, different field rates were applied to monitor the rate effect on the evolution of MFIS. Initially two cycles between zero and 16 kG were conducted with a field rate of 250 G/sec to stabilize the hysteresis loops. Then, the field rate was set between 25 G/sec and 500 G/sec and one cycle was recorded at each rate. In Figure 11, the response changes from one-step reorientation to two-step as the field rate decreases (Figure 12). The strain magnitude decreases from 5.2% to 4.6% as the rate decreases from 500 G/sec to 25 G/sec. Moreover, the magnetic hysteresis has a tendency to increase with the field rate.

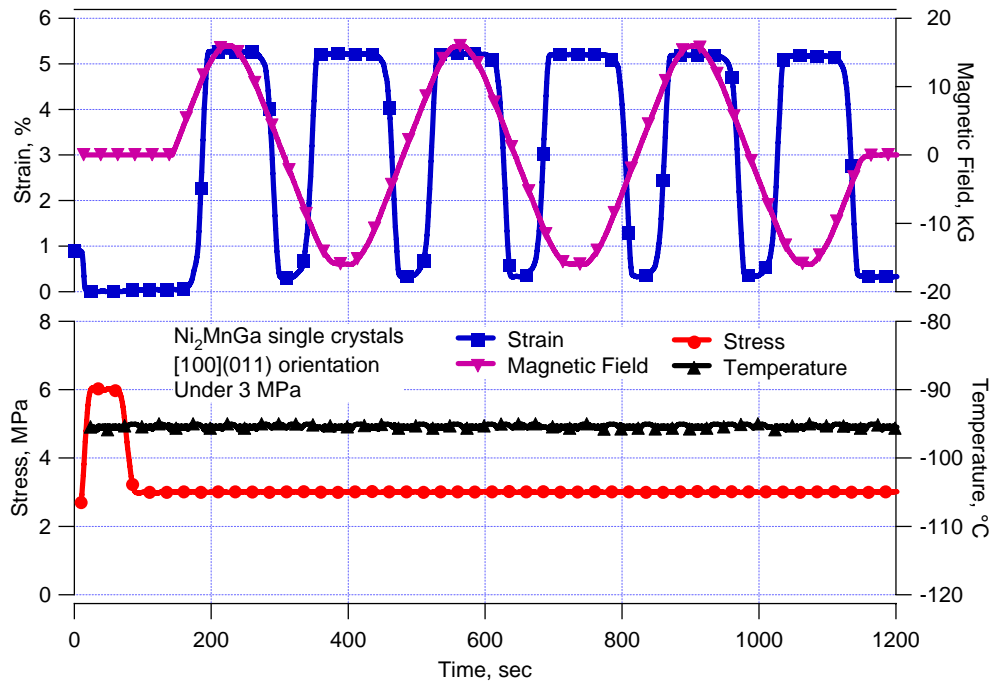


Figure 5. A plot of the representative data obtained during the MTM experiments. The stress is applied and kept constant, temperature is kept constant, magnetic field is ramped and strain response is measured.

iii. The stress induced martensite reorientation under constant magnetic field led to the observation of magnetoelasticity, i.e. recoverable martensite reorientation, similar to the pseudoelasticity due to the recoverable stress induced phase transformation in conventional shape memory alloys (Figures 13 and 14). The constant magnetic field caused an increase in the stress levels during reorientation, i.e. magnetostress. *The maximum magnetostress was 5.7 MPa in the present study, highest reported to date* (Figure 15).

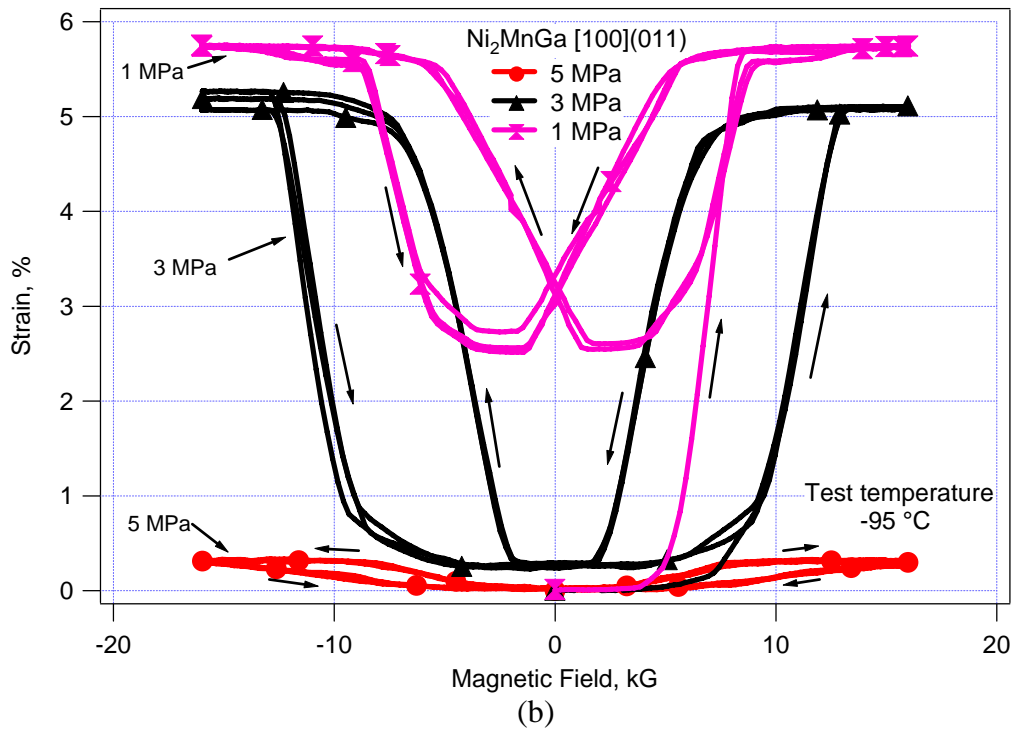
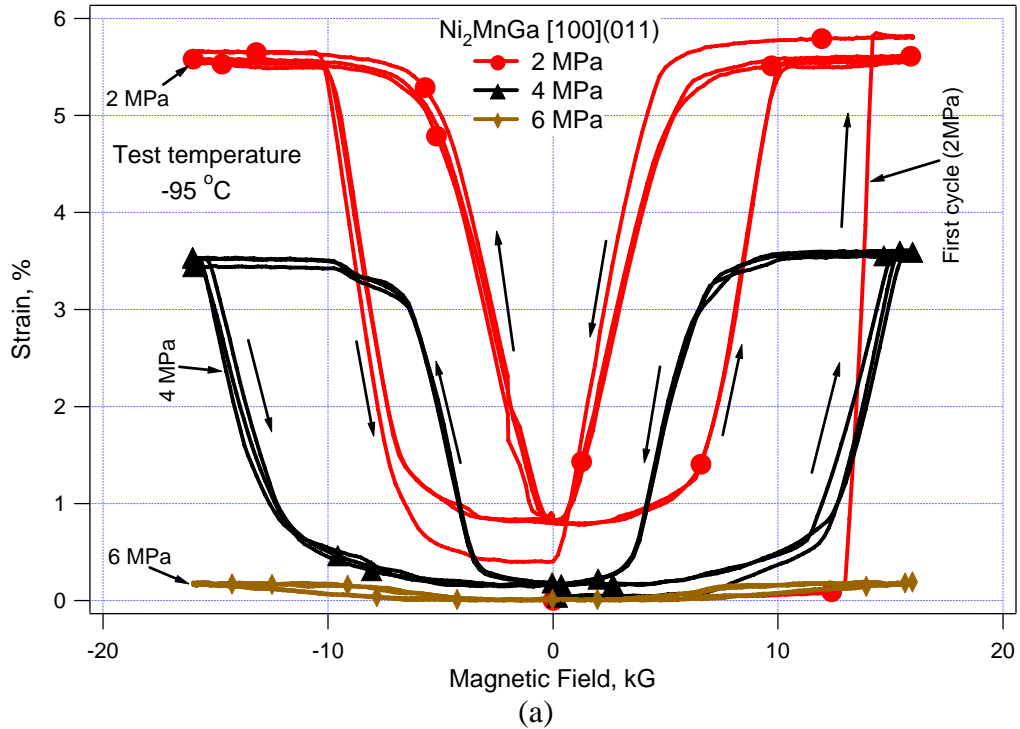


Figure 6. Evolution of strain in the Ni_2MnGa single crystals as a function of magnetic field under different constant compressive stress levels at $-95\text{ }^\circ\text{C}$. Three cycles are shown. a) Increased stress levels from 2 to 6 MPa, b) decreased stress levels from 5 MPa to 1 MPa. Only selected cases are shown for clarity.

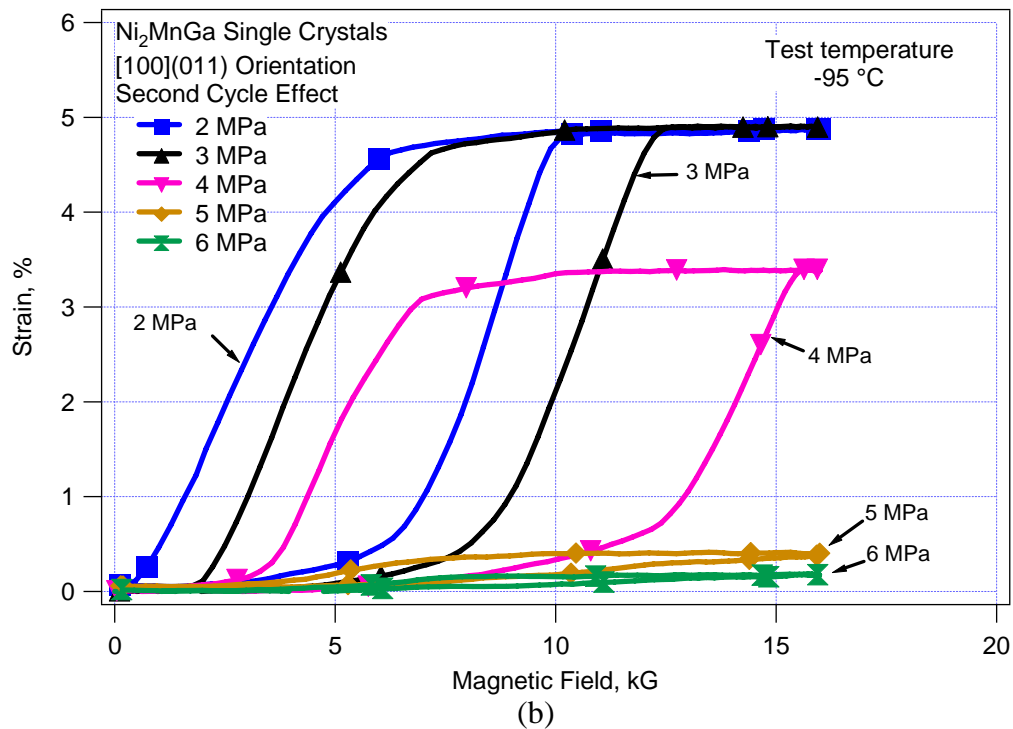
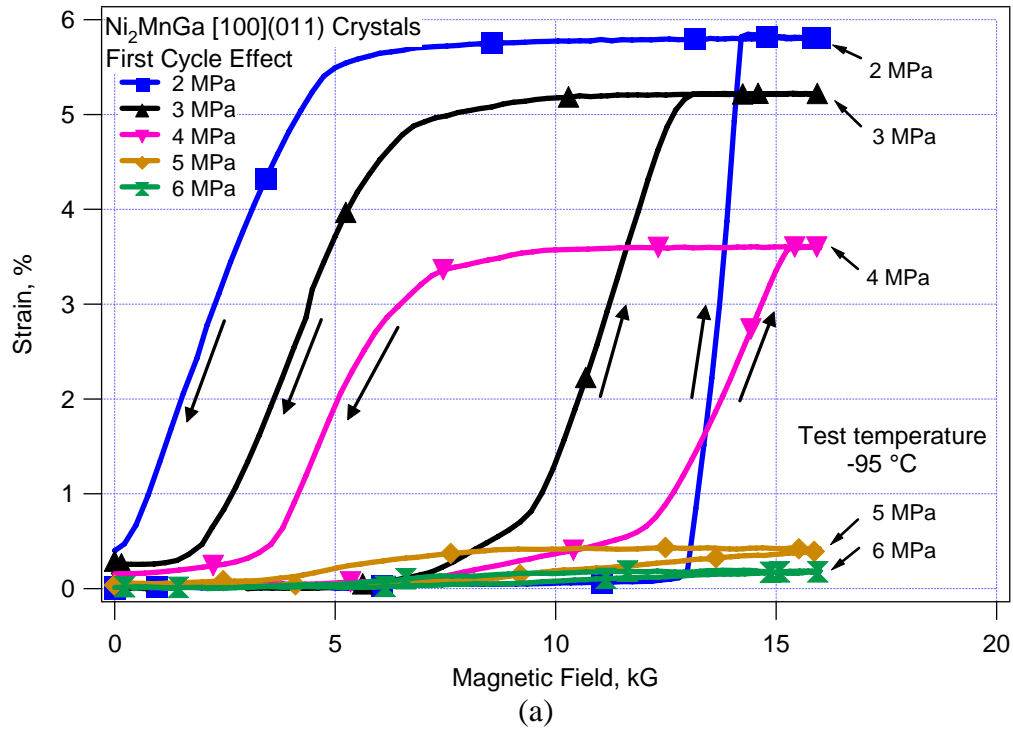


Figure 7. MFIS response during (a) first and b) second magnetic field cycles under constant stress levels.

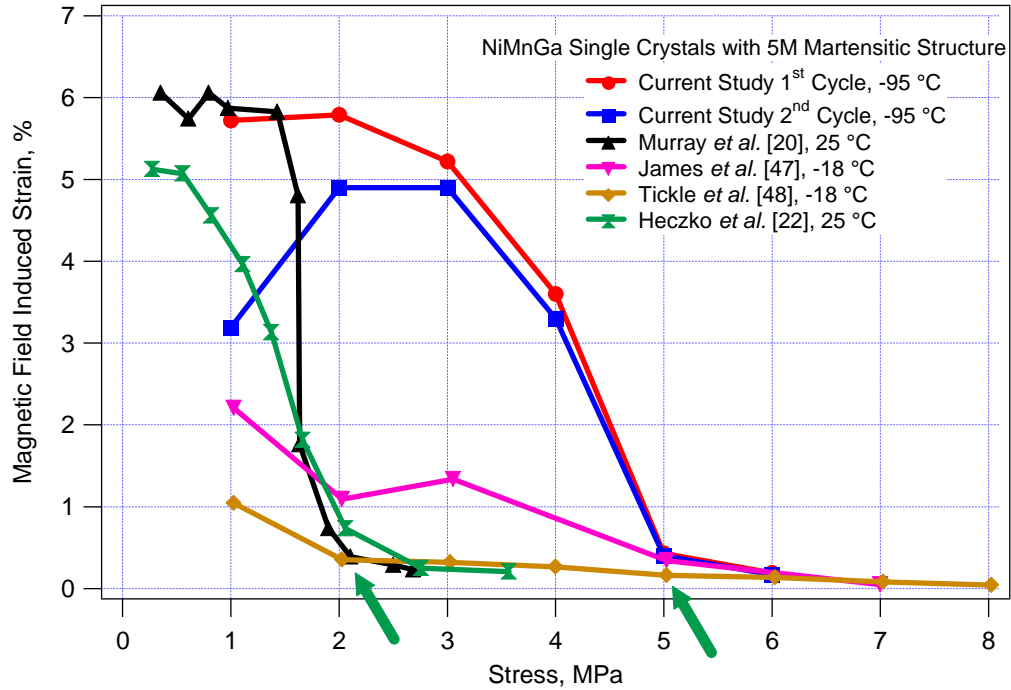


Figure 8. Magnetic field induced strain in the Ni₂MnGa single crystals of the present study for the first and second magnetic field cycles as a function of stress. Other magnetic field induced strain vs. stress curves published in literature are also included for comparison.

- iv. **The high magnetostress (5.7 MPa), high blocking stress (5 MPa) and the maximum MFIS (5.8%) combination observed is the highest reported to date for NiMnGa alloys with 5M martensite structure.** This was a consequence of both the large gap between the operating temperature (-95 °C) and the Curie temperature and the small difference between the operating temperature and the martensite start temperature. The former leads to increase in the magnetocrystalline anisotropy energy (Figure 16) and the latter provides low detwinning stress (Figure 17) which are what is needed to maximize the blocking stress and magnetostress. The magnetocrystalline anisotropy energy is calculated to be $3.30 \times 10^5 \text{ J/m}^3$ at -95 °C which was reported as $2.65 \times 10^5 \text{ J/m}^3$ at room temperature.
- v. **The critical field magnitudes under constant stress and the critical stress magnitudes under constant magnetic field for martensite reorientation follow a linear behavior** similar to the well-known Clausius-Clapeyron relationship between the applied stress and temperature for phase transformation in conventional shape memory alloys. The slope of this linear response is 1.8 kG/MPa (Figures 15 and 18) for both conditions which also surprisingly fit well to the previously reported data. This demonstrates the consistency of the present experiments and the material response in NiMnGa single crystals with 5M martensite structure. An empirical relationship between the applied stress and magnetic field for the onset of reorientation can be proposed considering the magnetocrystalline anisotropy energy, reorientation strain and saturation magnetic field as:

$$\frac{\Delta\sigma_m}{\Delta H} = \frac{K_u}{(H_s * \epsilon_0)} \quad (1)$$

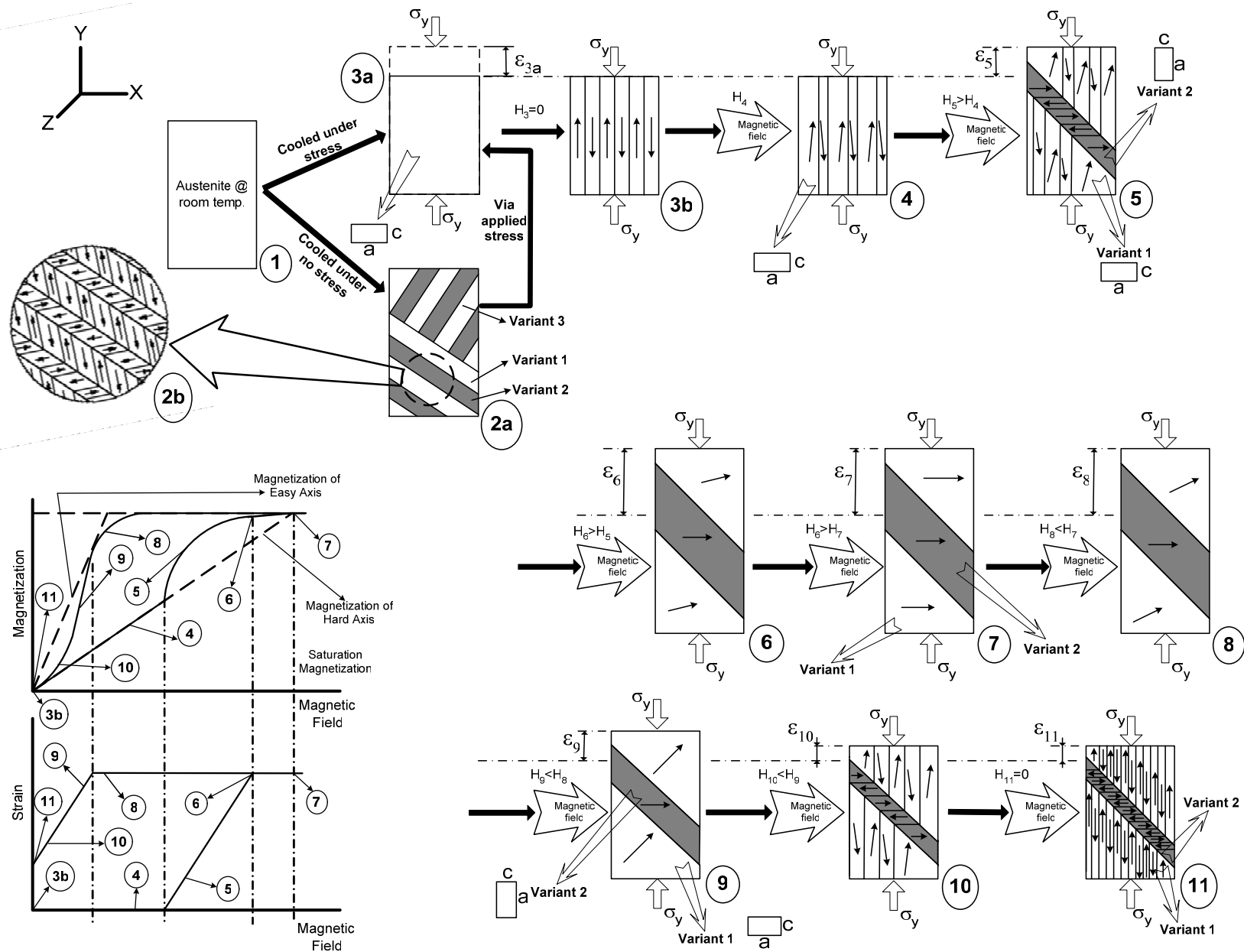


Figure 9. A schematic of the magneto- and microstructural mechanisms proposed to elucidate the evolution of magnetic field induced strain in different experimental conditions.

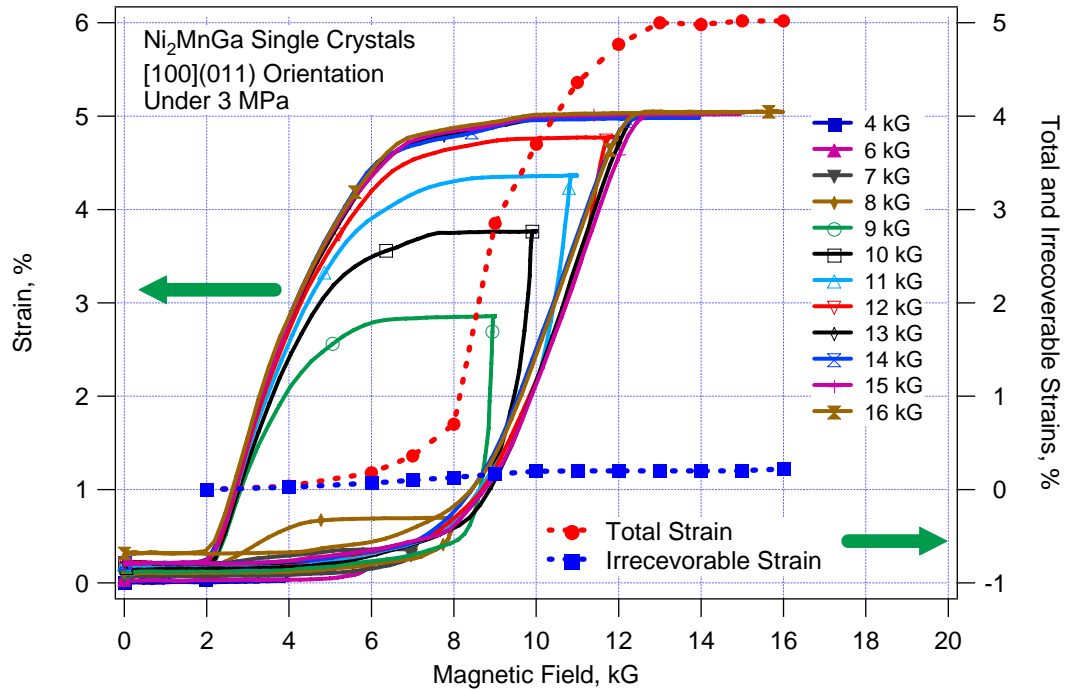


Figure 10. Incremental magnetic field response under a constant compressive stress of 3 MPa. Maximum and irrecoverable strain levels are shown on the right axis. The test temperature was -95 °C.

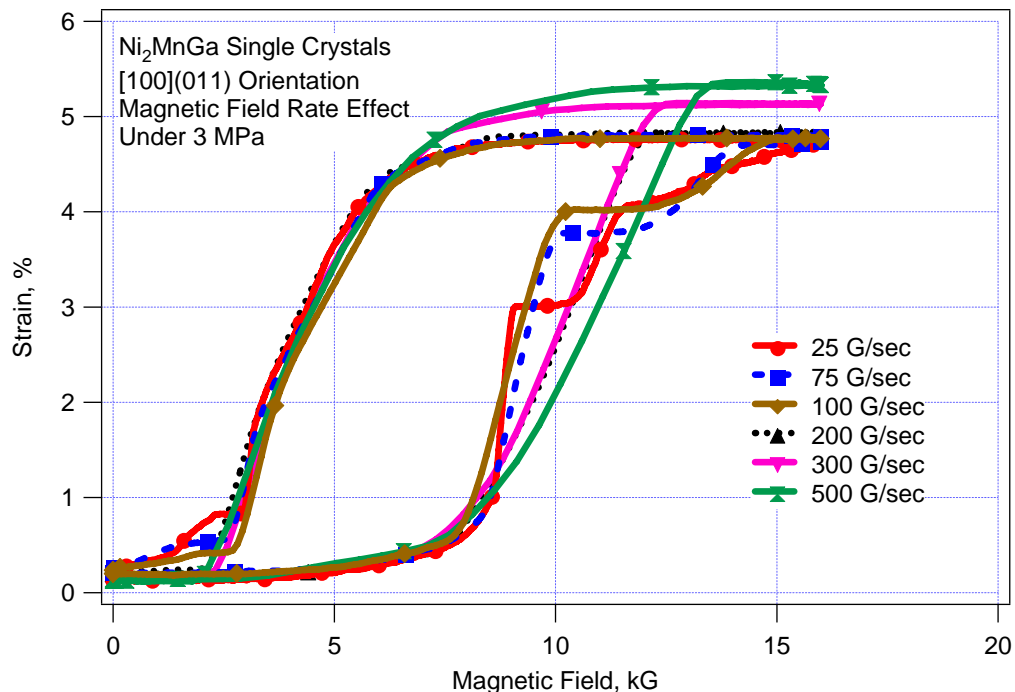


Figure 11. Effect of magnetic field rate on the MFIS evolution under 3 MPa showing two-stage reorientation. The test temperature was -95 °C.

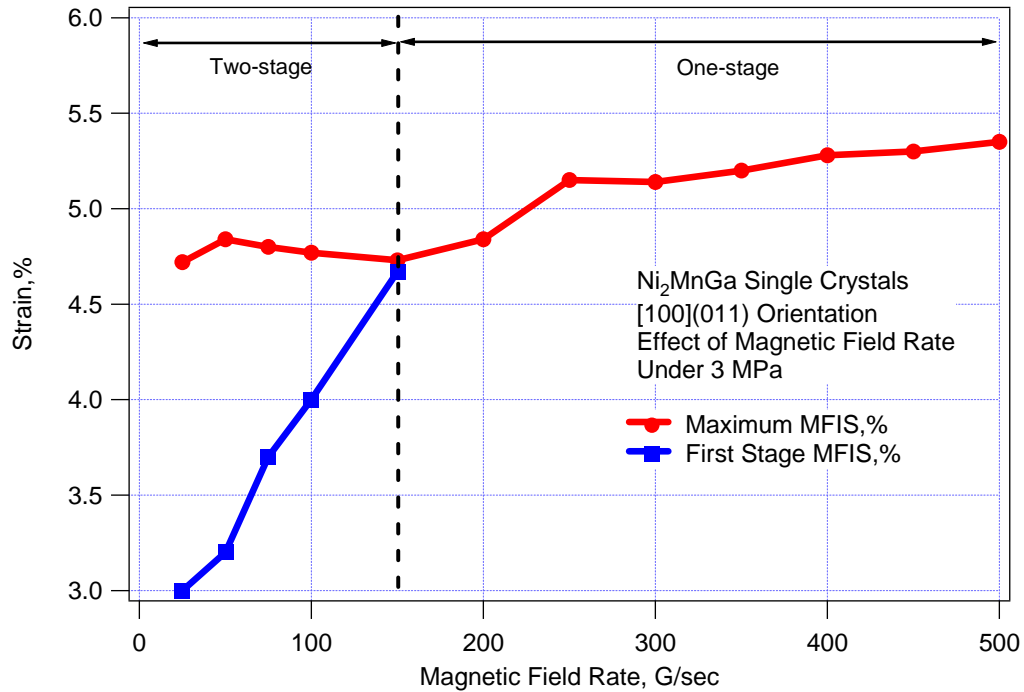


Figure 12. Effect of magnetic field rate on the MFIS magnitudes. The reorientation occurs in two stages for magnetic fields lower than 150G/sec and in one stage for higher rates.

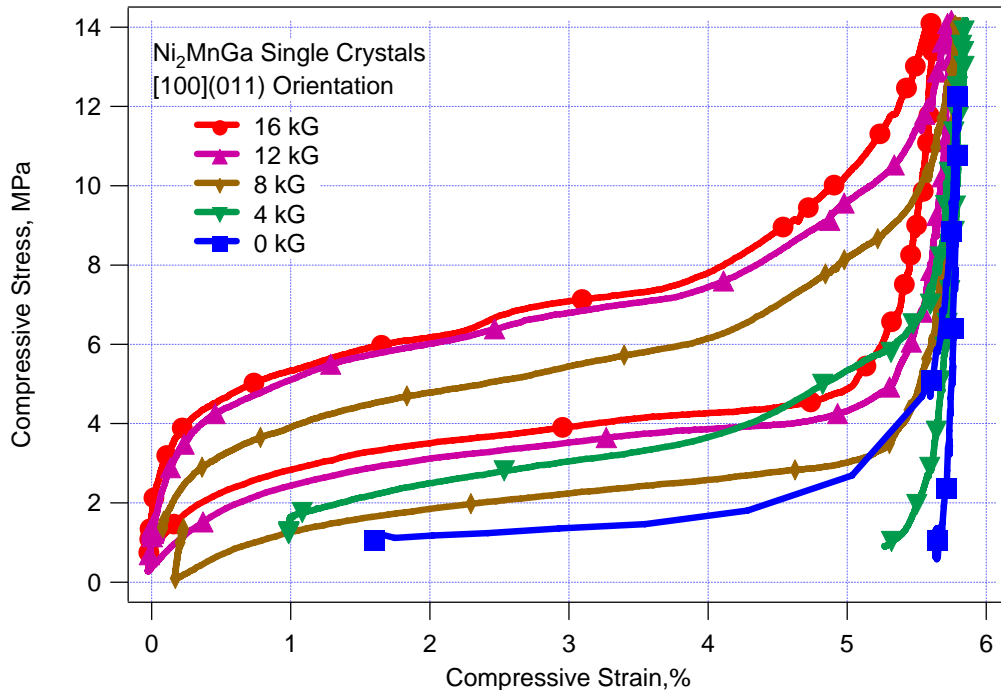


Figure 13. Effect of magnetic field on the stress-strain response the Ni_2MnGa single crystals during martensite reorientation. The test temperature was $-95\text{ }^\circ\text{C}$.

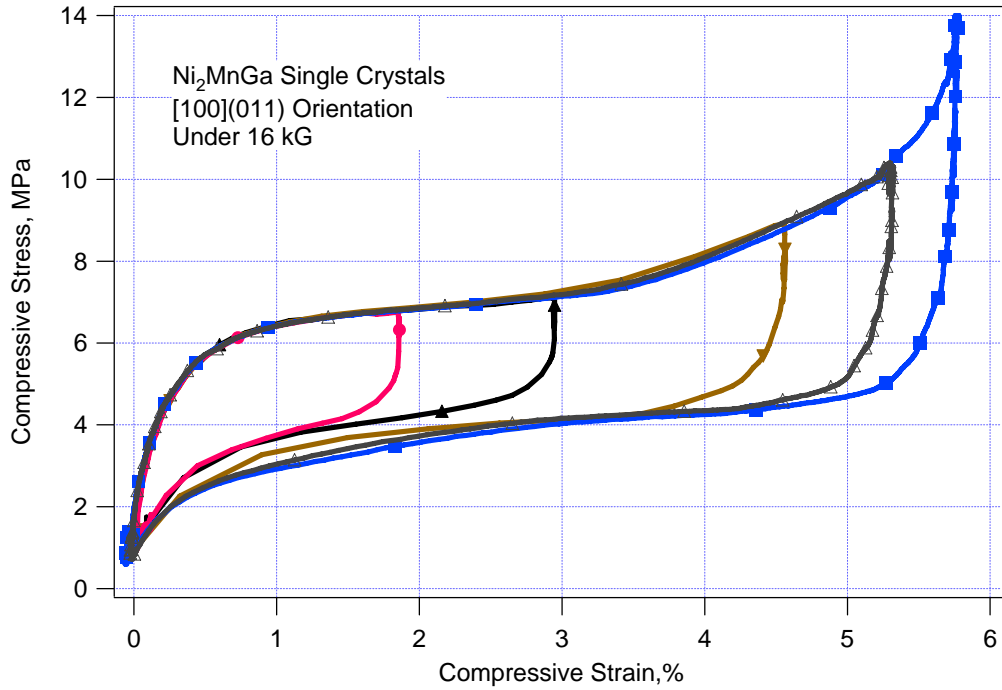


Figure 14. Stress-strain response of the Ni_2MnGa single crystals under a constant magnetic field of 16 kG. The loading was interrupted at selected strain levels for better understanding of strain and hysteresis evolution. The test temperature was -95°C .

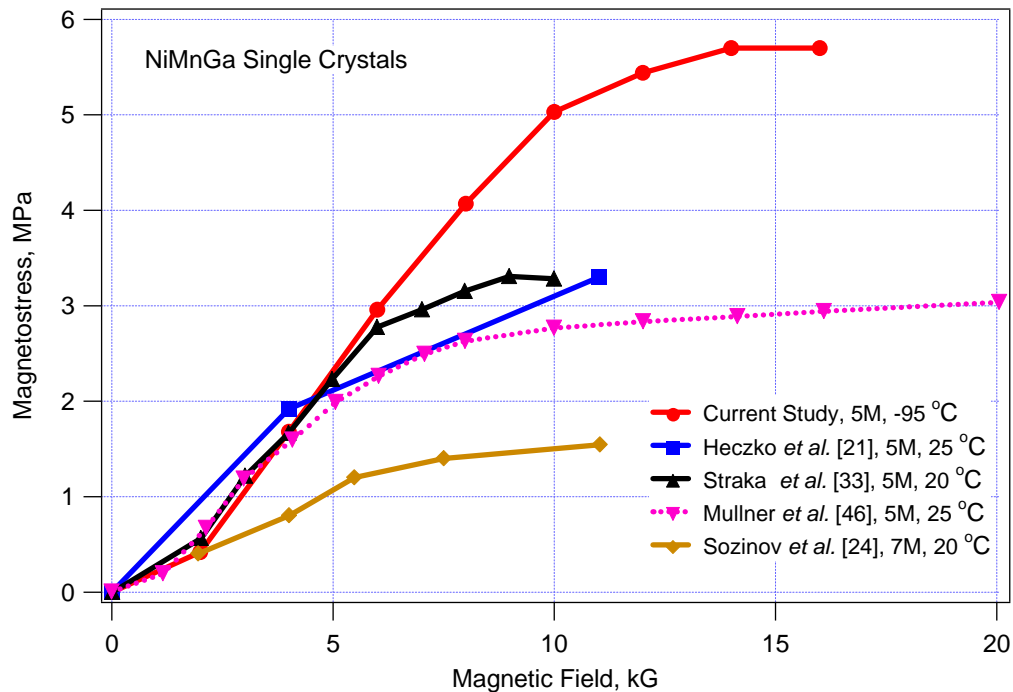


Figure 15. Magnetostress as a function of applied magnetic field for NiMnGa single crystals with different martensite modulation.

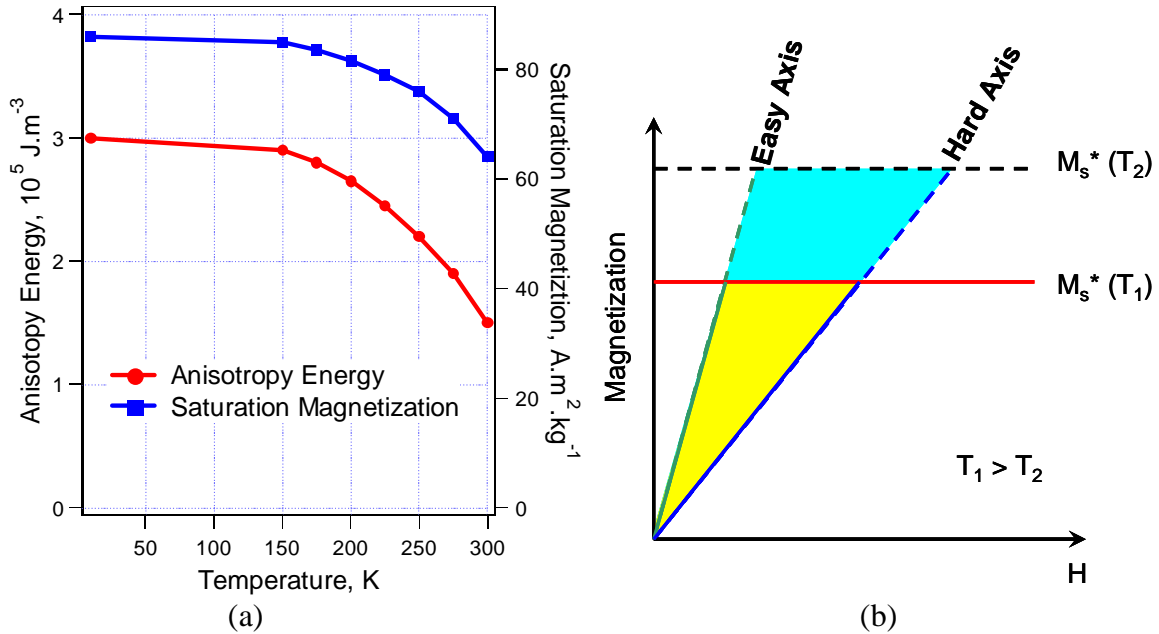
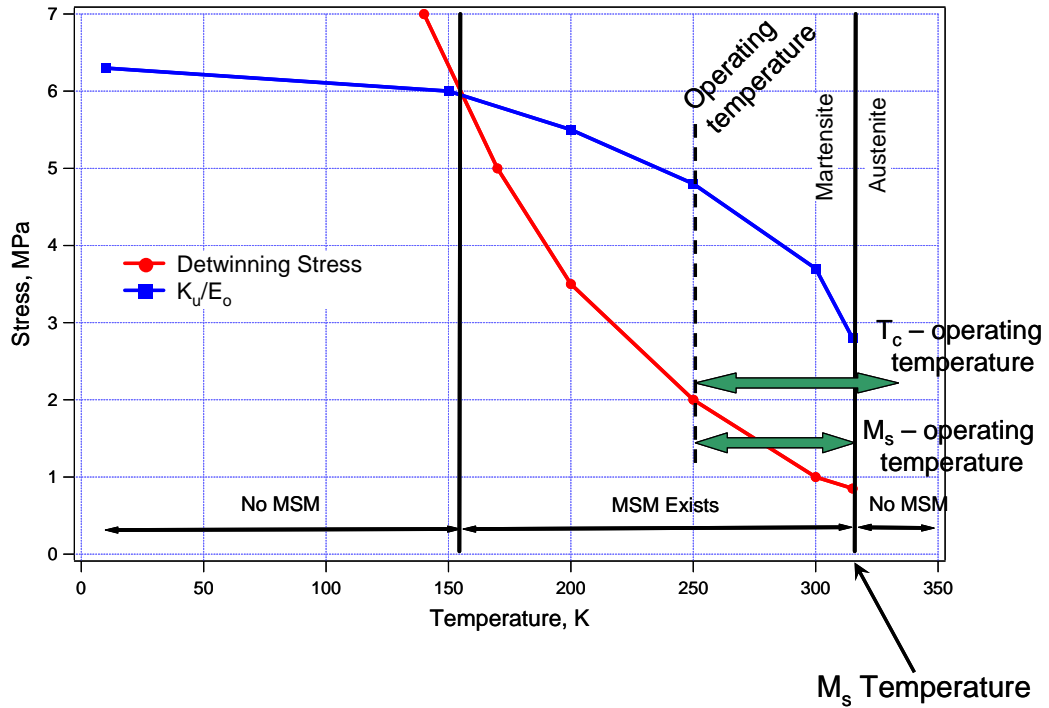
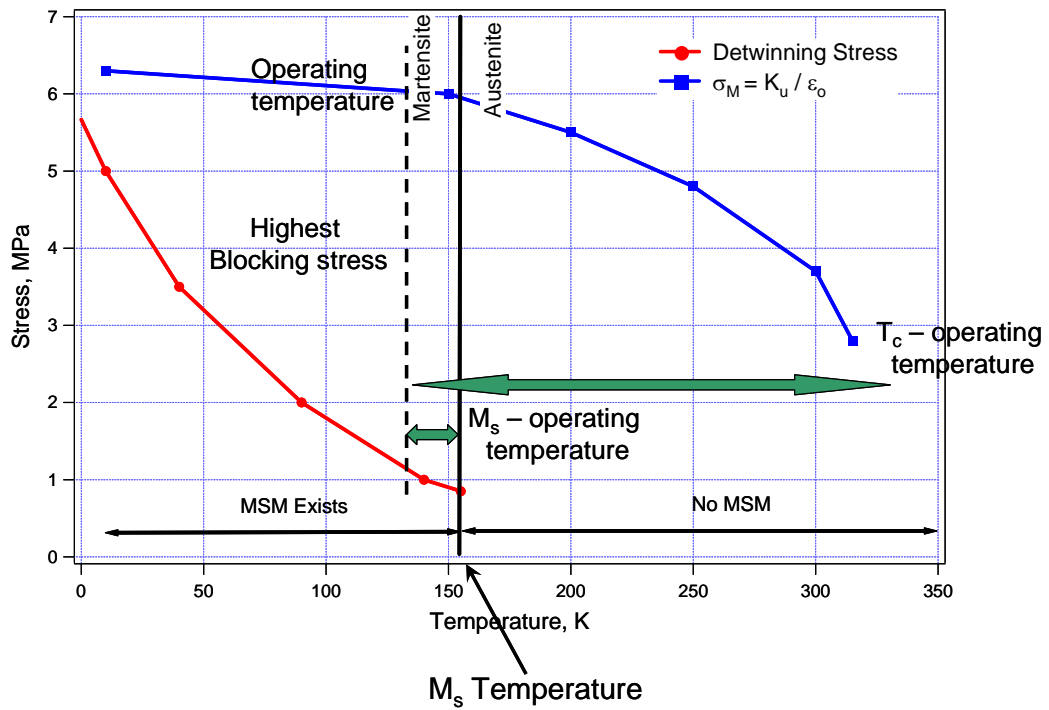


Figure 16. (a) Change in saturation magnetization and magnetocrystalline anisotropy energy with temperature in Ni₂MnGa alloys. (b) A schematic representation of the interrelationship between the saturation magnetization and anisotropy energy.



(a)



(b)

Figure 17. The effect of relative magnitude of martensite start (M_s), Curie (T_c), and operating temperatures (T_o) on the blocking stress. (a) Both $(T_c - T_o)$ and $(M_s - T_o)$ are large, (b) $(M_s - T_o)$ is minimized while $(T_c - T_o)$ is still large.

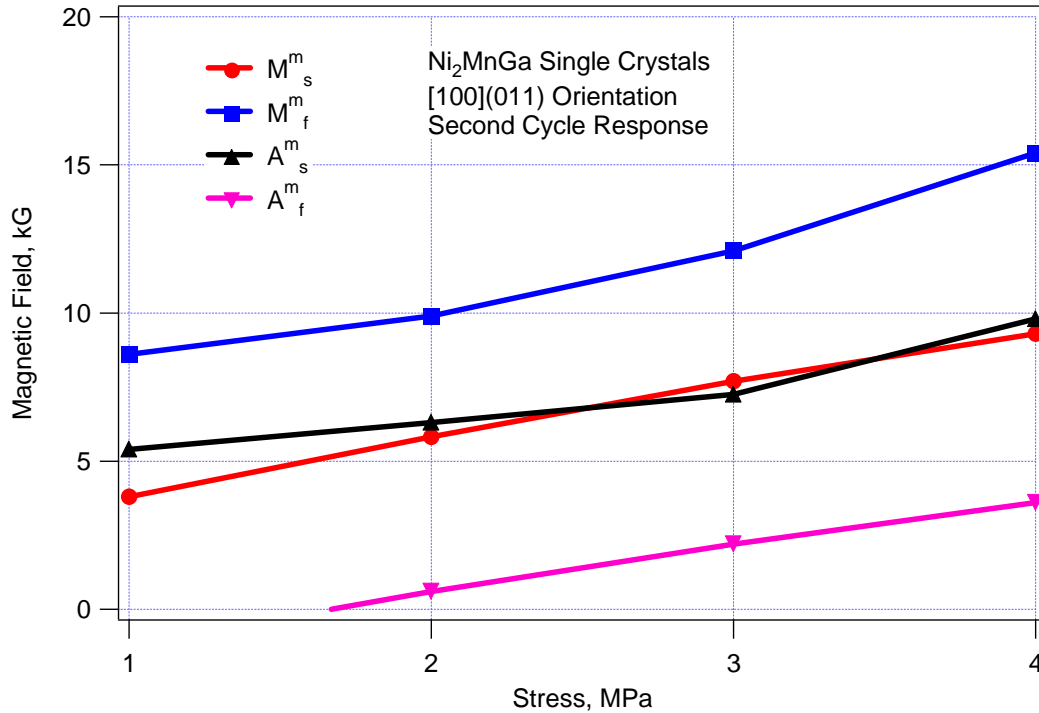


Figure 18. The change in the critical magnetic fields required for martensite reorientation as a function of stress.

5. We have also investigated the effect of magnetic field on the recoverable phase transformation in Ni_2MnGa single crystals. Here we reported for the first time that the field leads to cyclic forward and backward phase transformation under compression. Compressive stress and magnetic field were applied perpendicular to each other along the [100] and [011] axes, respectively. The applied magnetic field results in austenite stabilization and about **3.5% magnetic field induced strain via phase transformation** can be achieved under variable stress magnitudes depending on the testing temperature above A_s . The actuation stress achieved with this mechanism is about **24 MPa, one order of magnitude higher than what is reported before**. Additionally, for the first time in literature, 0.5% strain is recorded by cyclic magnetic field. The details related to the above findings can be summarized as follows:

- i. *Ni_2MnGa single crystals under compression along the [100] orientation demonstrated multistage stress-induced martensitic transformation in a certain temperature range* as shown in Figure 19. This is attributed to the intermartensitic phase transformation. Figure 20 shows the superelastic response of the first-stage transformation as a function of temperature. The critical stress for transformation, transformation strain and stress hysteresis decrease with temperature. For temperatures above -40°C , first-stage transformation does not occur. The two stage transformation is determined to be L_{21} parent to orthorhombic martensitic to 5M tetragonal martensitic transformations using high energy XRD with synchrotron radiation (Figure 21). The peak at 4.2° corresponds to the $[004]_{L_{21}}$ plane, while the peaks at 3.74° , 4.16° and 4.63° correspond to the [022], [220]

and [004] planes of tetragonal martensite, respectively. An additional smaller peak forming and disappearing at 3.9° is due to the orthorhombic martensitic phase.

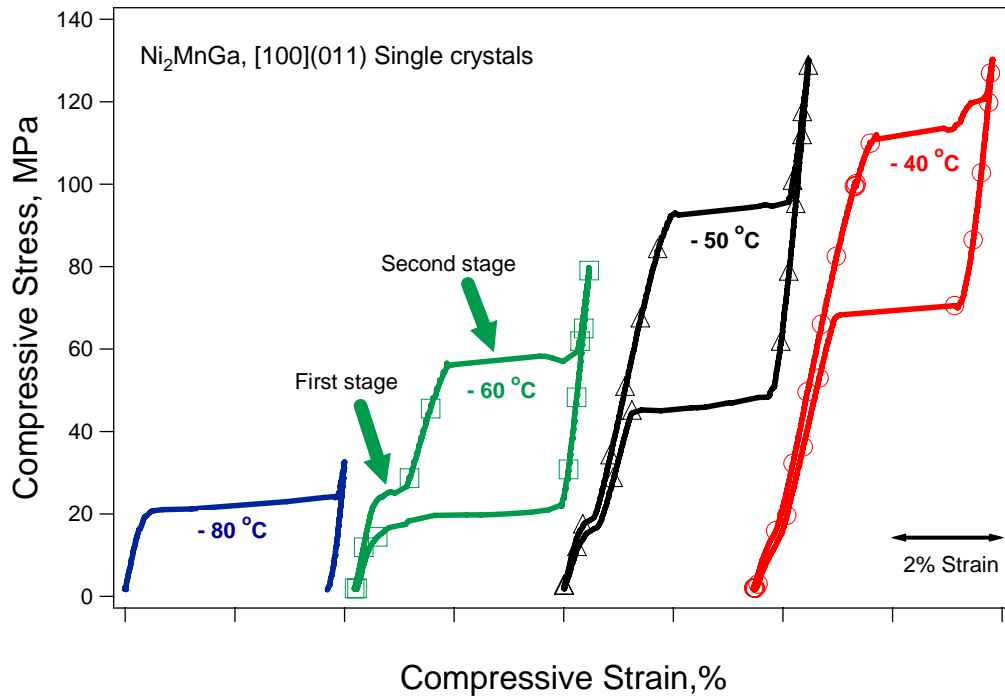


Figure 19. Pseudoelastic response of Ni_2MnGa single crystals as a function of temperature under compression along the [100] orientation. The critical stress for inducing transformation increases with temperature for the second stage while it decreases for the first stage.

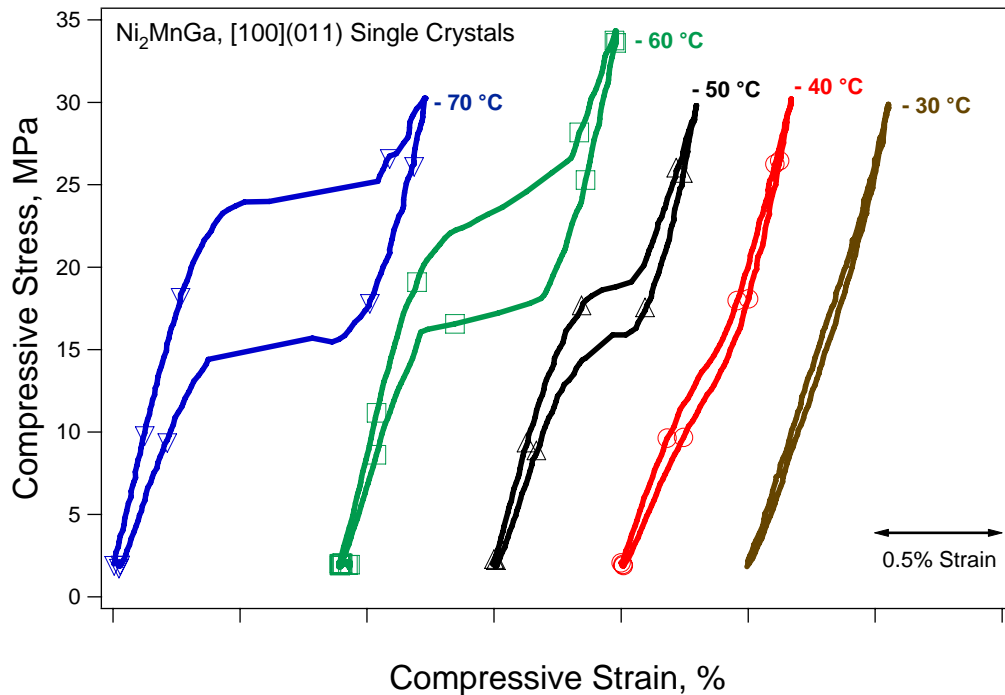


Figure 20. First stage pseudoelastic response of Ni_2MnGa single crystals as a function of temperature under compression along the [100] orientation.

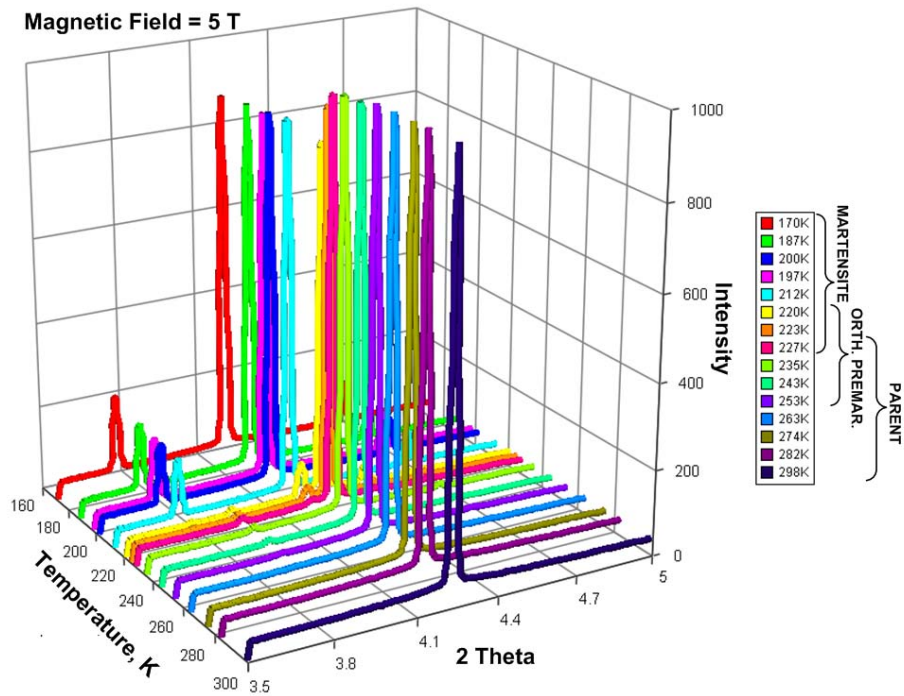


Figure 21. Temperature range in which multi-stage phase transformation is observed and accompanying phases detected using high energy XRD with synchrotron radiation.

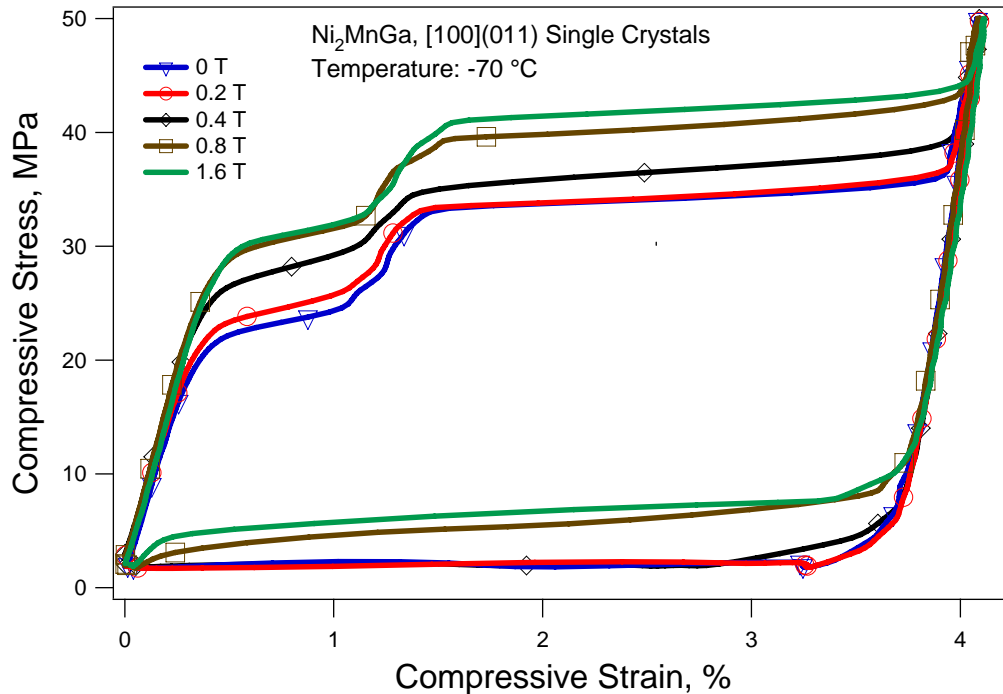


Figure 22. Effect of magnetic field on the pseudoelastic response of the Ni₂MnGa single crystals at -70 °C. The critical stress levels for inducing phase transformation increase with field up to a critical level and saturate at higher fields.

ii. The constant applied magnetic field perpendicular to the stress direction increases the critical stress magnitudes for phase transformations (Figure 22). At all temperatures, the magnetic field shifts the stress required to induce phase transformation to higher levels without affecting the stress hysteresis. Critical stress magnitudes for the first and second stages are increased by 7.5 MPa and 10.5 MPa, respectively. It can be concluded from this figure that 0.8 T is sufficient for the saturation of the stress increase for the first stage where magnetic field close to 1 T is needed for the saturation of the stress increase in the second stage. During unloading, under no magnetic field there is no back transformation while unloading under applied magnetic field of 0.5, 1 and 1.6 T resulted in back transformation from martensite to austenite at 2, 3 and 4 MPa respectively. It can be concluded that 3.8 % magnetic field induced martensite to austenite phase transformation strain is evident observed in Figure 21. **This is the first time where magnetic field induced fully recoverable pseudoelasticity is reported.** In the first stage transformation (Figure 23), an observation, which has implications for the reversible field-induced phase transformation, is that at temperatures above -60°C , the critical stress for the reverse transformation under 1.6 Tesla is higher than the critical stress for the forward transformation under zero magnetic field. In other words, pseudoelastic loops with and without magnetic field are separable since the stress hysteresis at zero field is low and the increase in the critical stress level due to the magnetic field (i.e. magnetostress = $\sigma_{c,forward}^H - \sigma_{c,forward}$) is larger than the stress hysteresis.

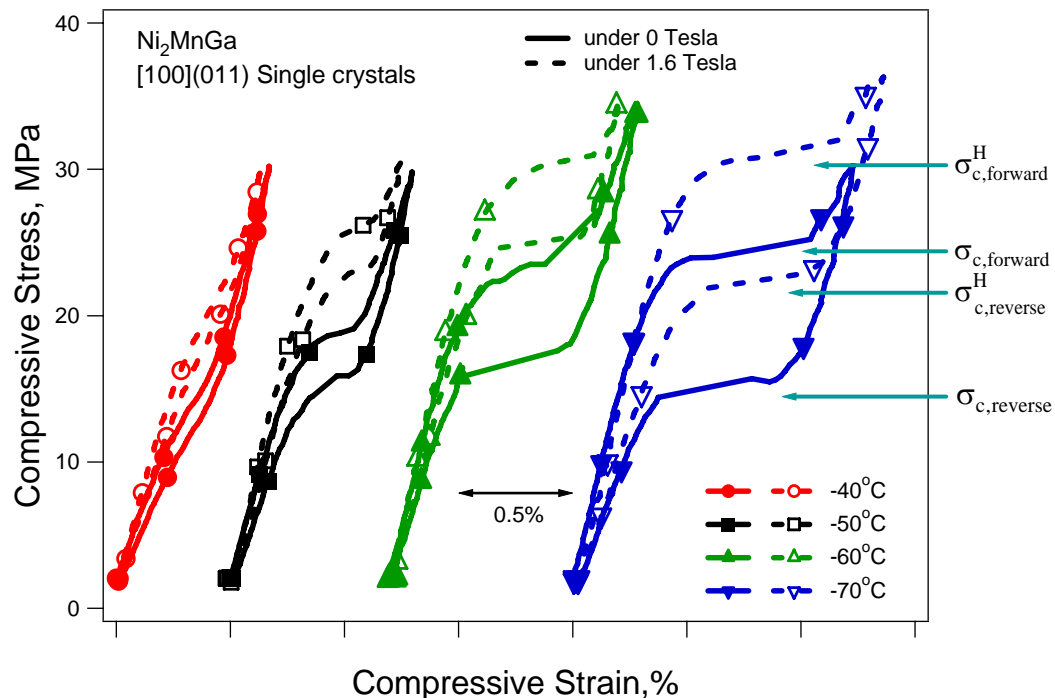


Figure 23. Temperature and field dependence of the critical stress levels and stress hysteresis during the first stage transformation. Transformation stress, strain and stress hysteresis decreases with increasing temperature. Solid lines demonstrate the response under zero magnetic field while the dotted lines show the one under 1.6 Tesla.

iii. It was also possible to induce martensite to austenite phase transformation after the formation of stress induced martensite upon loading in the first stage. Figure 24.a demonstrates an example with accompanying MFIS vs. magnetic field response (Figure 24.b) at -55 °C. The stress was increased up to point 1 ($>\sigma_{c,forward}$) leading to parent to orthorhombic martensite phase transformation and then unloaded to point 2 ($<\sigma_{c,reverse}^H$) under zero field. At point 2, the stress was kept constant at 22 MPa and the field was applied, which triggers the reverse transformation to the parent phase at around 0.7 Tesla in the first cycle and at 0.5 Tesla in the following cycles. Switching the field on and off continuously induces forward and reverse phase transformation without significant change in the field magnitudes (points 3,4,5, and 6). Thus, ***the field can do work against stress levels above 20 MPa indicating one order magnitude increase in actuation stress with respect to magnetic field induced reorientation in MSMA's.*** The field-induced strain was only about 0.5% because of the low transformation strain along the [100] orientation accompanying the parent to martensite transformation. If the stress is reduced incrementally, the field required to trigger the forward and reverse transformations decreases. And at 18 MPa (point 7), the field can only induce reverse transformation at 0.2 Tesla because the stress level is lower than $\sigma_{c,forward}$.

iv. ***It is possible to accomplish a one-way shape memory effect in the second stage phase transformation.*** Figure 25 shows the stress-strain-magnetic field response during the second stage transformation at -60 °C demonstrating the field-induced one way shape memory effect. The sample was loaded up to 64 MPa under 1.6 Tesla (point 1), below $\sigma_{c,forward}^H$ but above $\sigma_{c,forward}$, and then the magnetic field was reduced while keeping the stress constant. The forward phase transformation took place resulting in a 2.4% strain (point 2) as the magnetic field was reduced from 0.7 to 0.5 T. Although the reapplication of the field did not trigger reverse transformation at this stress level (point 3), a decrease in stress or increase in temperature would result in the reverse transformation. After the forward transformation, the sample was unloaded to 24 MPa (point 5) under zero field, i.e. to a stress level between $\sigma_{c,reverse}^H$ and $\sigma_{c,reverse}$. Then, the magnetic field was applied resulting in 3.1 % MFIS (point 6) due to the reverse transformation at the field magnitudes of 0.1 to 0.6 Tesla. When the magnetic field was cycled between 0 to 1.6 Tesla at 24 MPa, a cyclic MFIS of 0.3% was observed due to the reversible field-induced parent to orthorhombic martensitic phase transformation. Unloading the sample under 1.6 Tesla completes the pseudoelastic cycle (point 9). This demonstrates that in one pseudoelastic cycle it is possible to activate both reversible and irreversible field-induced phase transformation depending on the stress level.

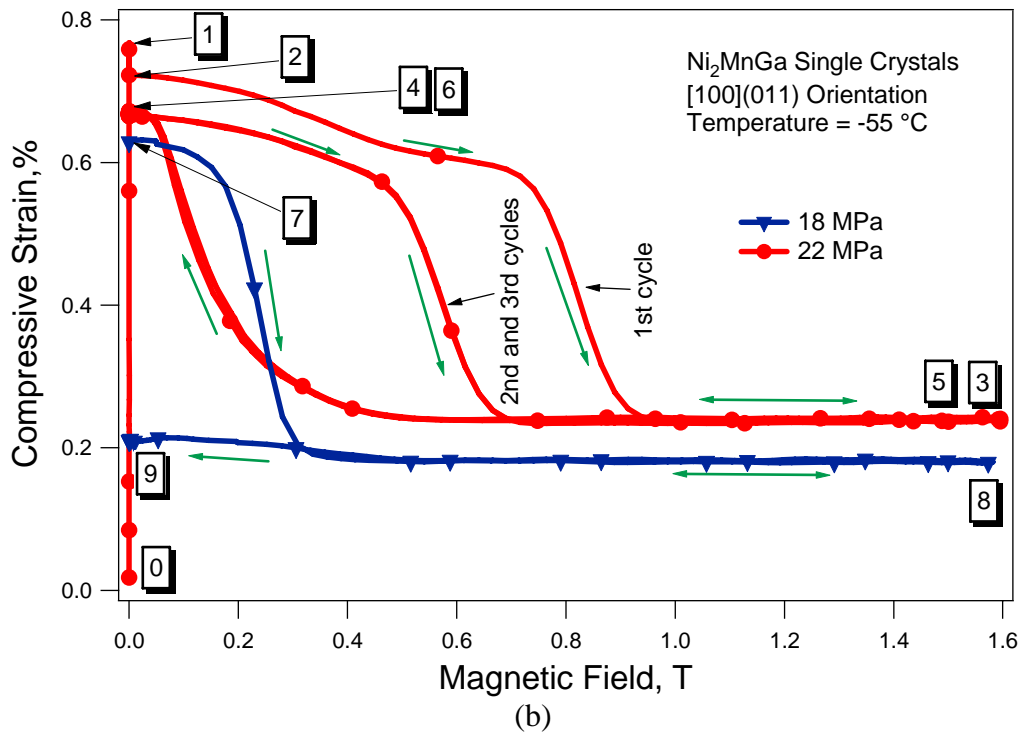
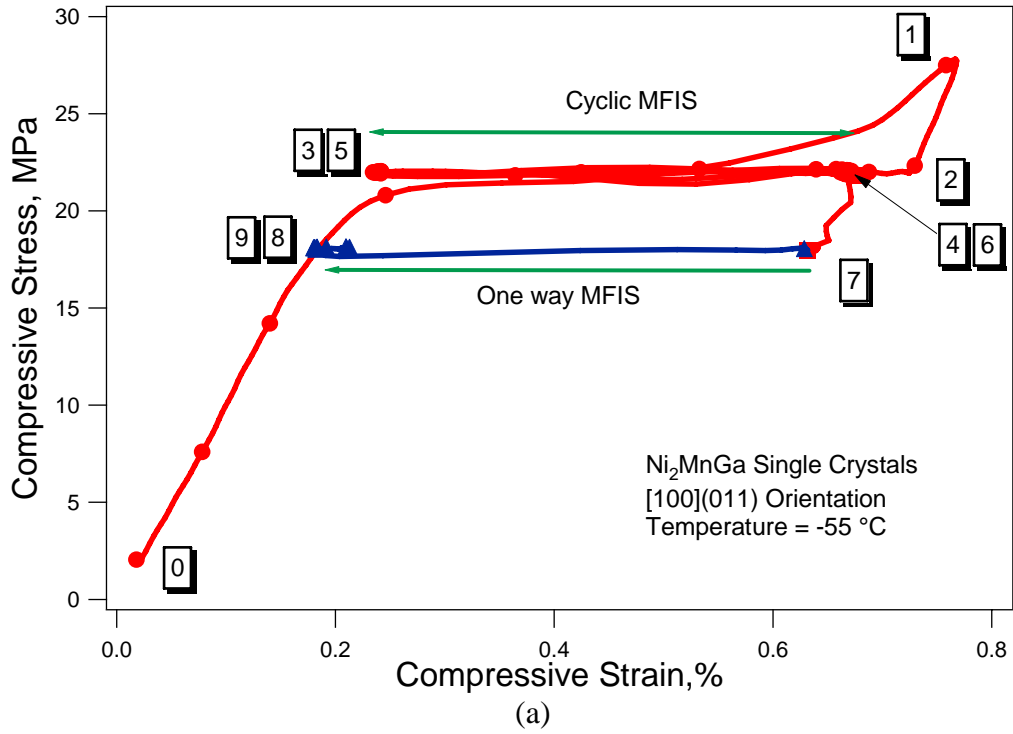


Figure 24. Demonstration of reversible field-induced phase transformation at low field magnitudes. Data in (a) and (b) are from the same experiment. The number sequence demonstrates the loading path.

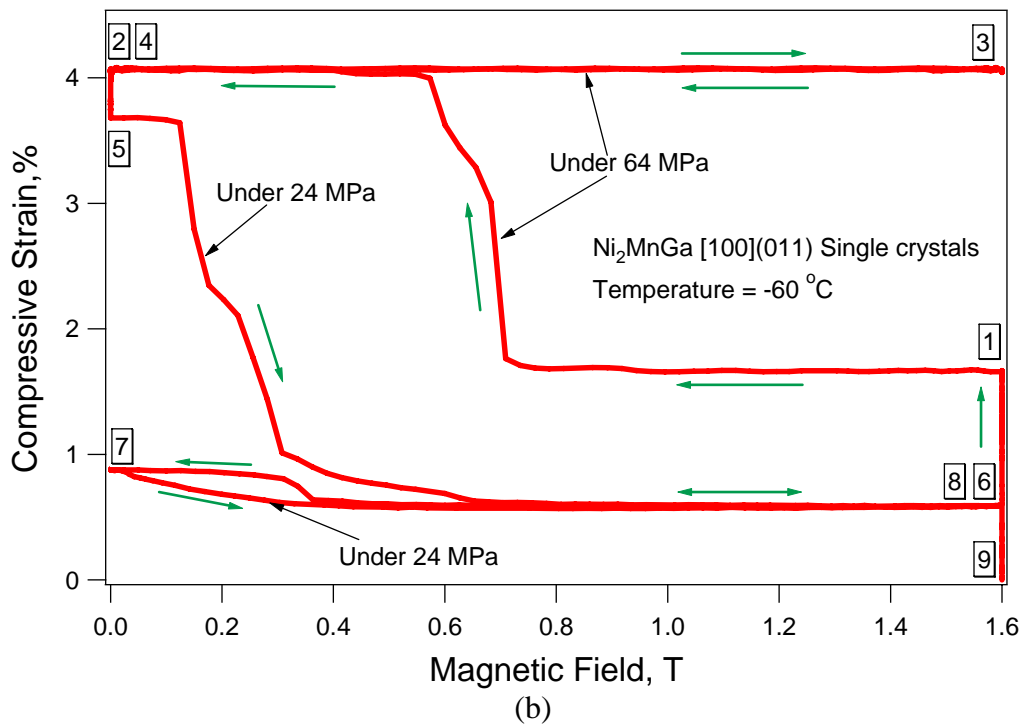
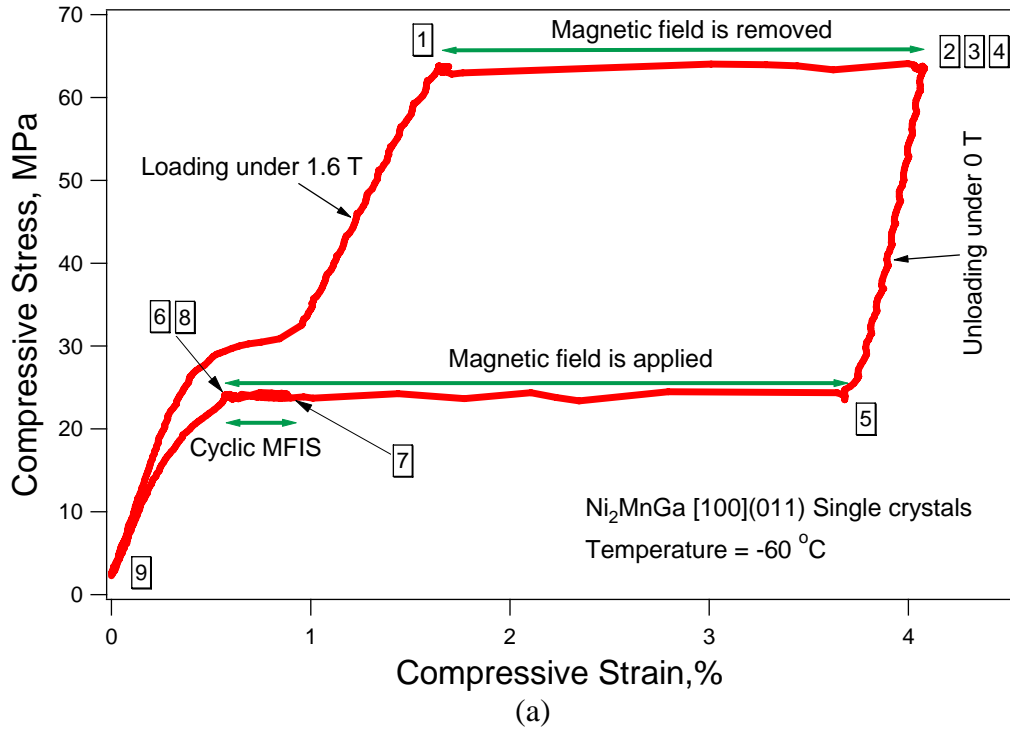


Figure 25. Demonstration of field-induced one way shape memory effect via orthorhombic to 5M tetragonal martensitic transformation or vice versa at low field magnitudes. Note the high actuation stress level with significant MFIS. Data in (a) and (b) are from the same experiment. The number sequence demonstrates the loading path.

7. *CoNiAl polycrystal samples demonstrated perfect superelastic behavior, large temperature window for pseudoelasticity (>200 °C), more than 4% fully recoverable transformation strains, more than 3.2% two way shape memory (TWSME) strain without any thermomechanical training and large difference between stresses required for martensitic transformation and for dislocation slip* (Figures 26-29). Because of these properties, *this material is a potential candidate material for both conventional and magnetic shape memory applications* and its properties need to be exploited in great detail. To the best of our knowledge, this work is the first study that investigates both conventional and magnetic shape memory behavior of CoNiAl alloys.

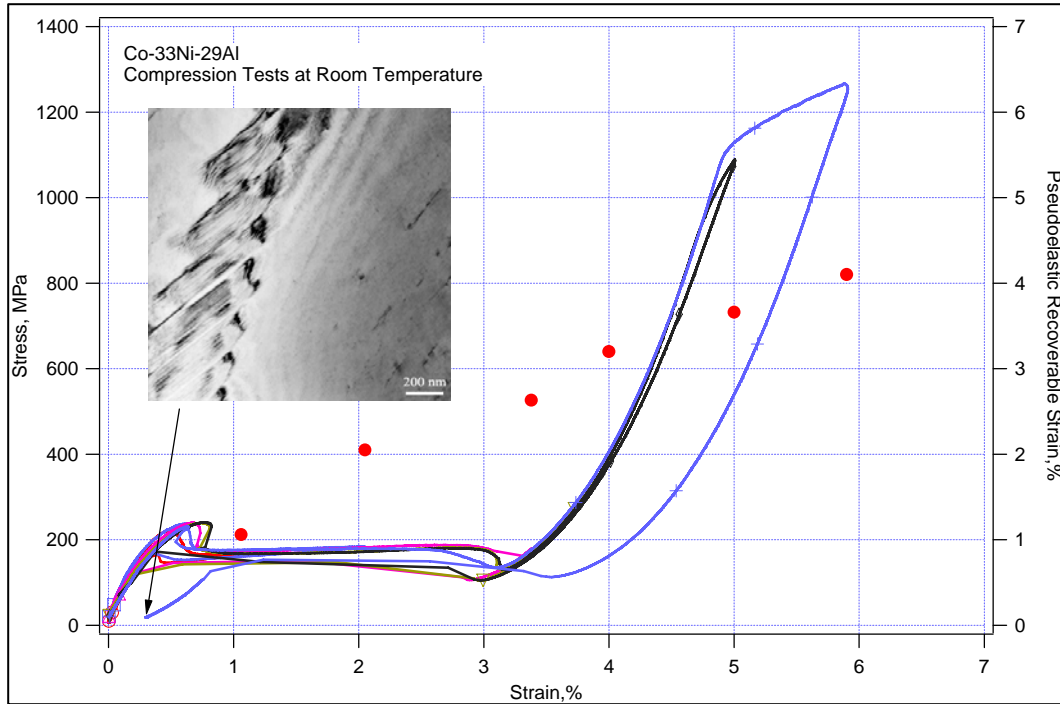


Figure 26: Compressive stress vs. applied strain and recoverable strain vs. applied strain response of Co-33Ni-29Al (at%) polycrystals at room temperature. The TEM image in the inset figure shows deformation twins formed at the second plateau which caused small irrecoverable strain shown in the figure.

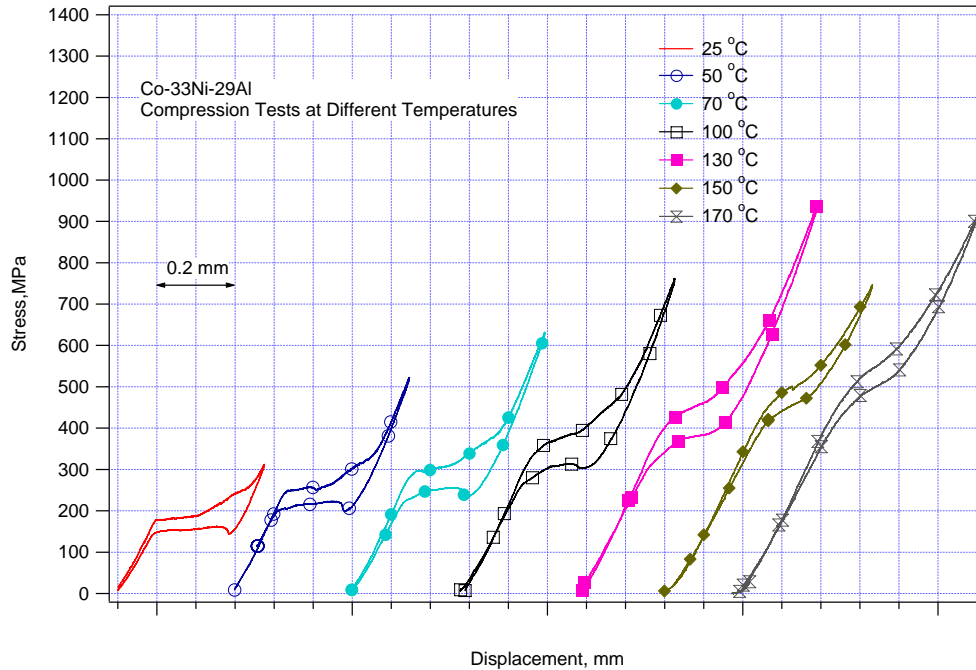


Figure 27: Compressive stress vs. applied strain response of Co-33Ni-29Al polycrystals at different temperatures.

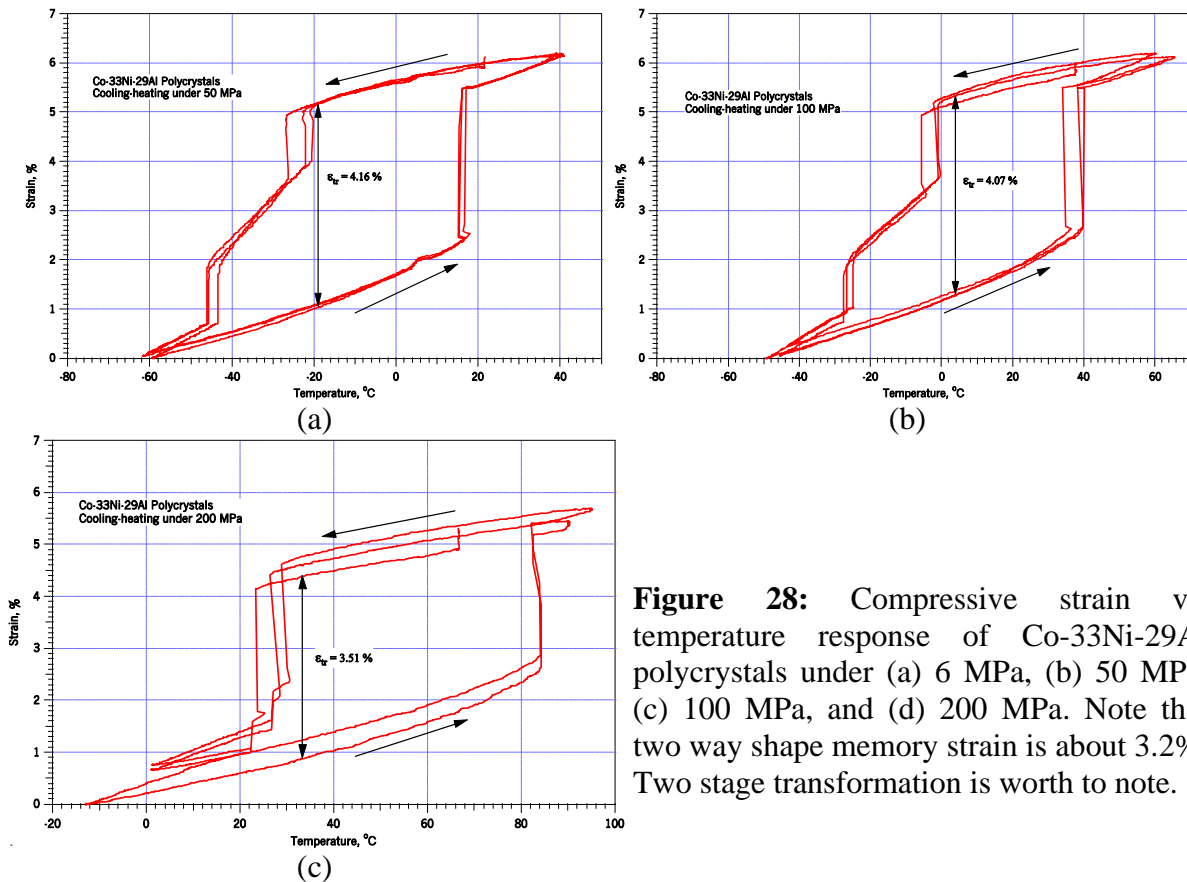


Figure 28: Compressive strain vs. temperature response of Co-33Ni-29Al polycrystals under (a) 6 MPa, (b) 50 MPa, (c) 100 MPa, and (d) 200 MPa. Note that two way shape memory strain is about 3.2%. Two stage transformation is worth to note.

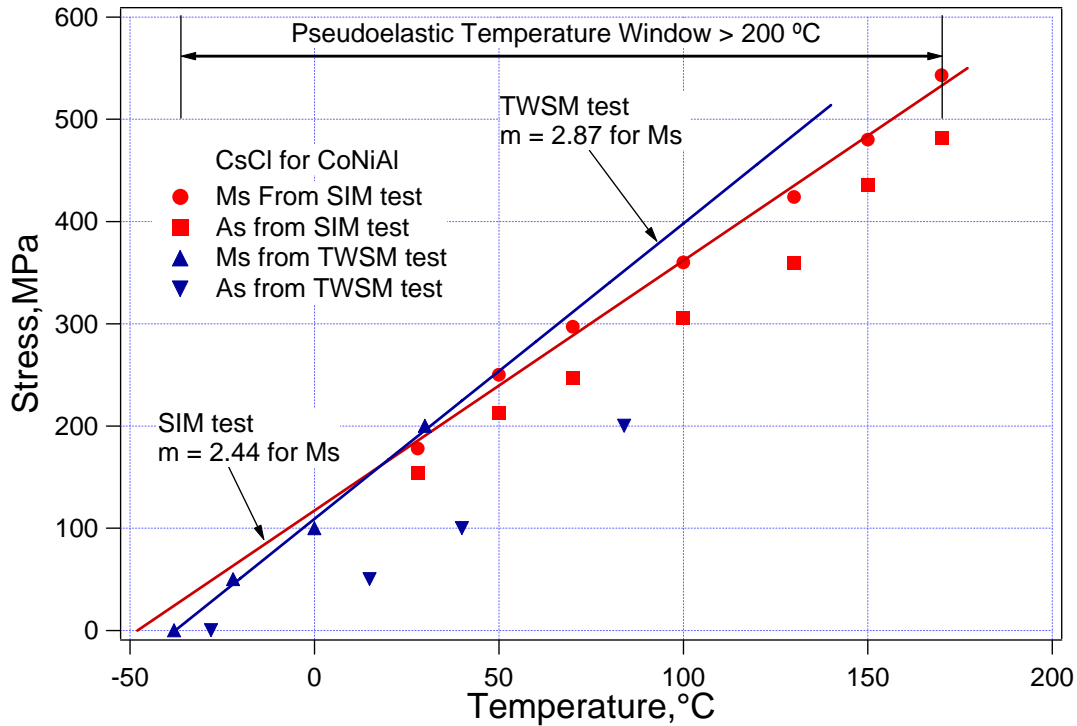


Figure 29: The Classius-Clapeyron Curve for the present Co-33Ni-29Al polycrystals. The figure shows variation of martensite forward and backward transformation stresses as a function of temperature obtained from experiments in Figure 27 and variation of Ms and As temperatures as a function of applied stress obtained from experiments in Figure 28. The solid lines were fit the latter data. SIM: Stress induced martensite, TWSM: Two way shape memory.

8. **Further advantages of CoNiAl alloys under investigation can be summarized as follows.** In CoNiAl alloys, Curie temperature (T_c) and Ms temperature change independently with composition as opposed to other magnetic shape memory alloys (MSMAs) such as NiMnGa in which T_c is rather constant. CoNiAl alloys are cheaper when compared to other MSMAs such as NiMnGa and FePd. They have higher magnetocrystalline anisotropy energy (3.9×10^6 erg/cm³) as compared to NiMnGa (2.0×10^6 erg/cm³). We have demonstrated formation of FCC second phase with appropriate heat treatments mostly along grain boundaries and also grain interiors such that these alloys does not suffer from brittleness problem that NiMnGa and other NiAl based alloys suffer. CoNiAl alloys have excellent oxidation and corrosion resistance, low density and high melting points.
9. **CoNiAl alloys are also potential high temperature shape memory alloys (HTSMA)** since Ms temperature can be as high as 170 °C or may be higher but it needs further investigation. The thermal hysteresis is considerably smaller than other known HTSMAs such as CuNiAl, NiTiHf and NiTiPd. We have demonstrated that **CoNiAl alloys have excellent fatigue behavior** as compared to CuNiAl and NiTi. As compared to CuNiAl, the microstructure is more stable since the precipitation temperatures are very high.
10. Compressive and tensile response of the CoNiAl single crystals along different crystallographic orientations revealed that transformation strains (and also pseudoelastic

strains) are 4.2 % in the [100], 2.5% in the [123] and almost 0% in the [111] orientations under compression (Figures 30-34). On the other hand, **both transformation and pseudoelastic strain levels are as high as 10% in tension** (Figure 35). This is attributed to the ease of detwinning under tension similar to NiTi alloys. Figure 36 shows the tensile test results of [110] oil quenched single crystals. It is noteworthy to mention that only 9 MPa is sufficient for single martensite variant formation with low temperature hysteresis as further increase in stress level does not change the transformation stress level significantly (Figure 36.a). Figure 36.b shows the pseudoelastic response at different temperatures. Perfect pseudoelastic behavior up to 250 °C makes CoNiAl alloys a promising high temperature shape memory alloy. Incremental pseudoelastic strain test at 220 °C is shown in Figure 36.c. Stress hysteresis is about 150 MPa and does not strongly depend on strain levels.

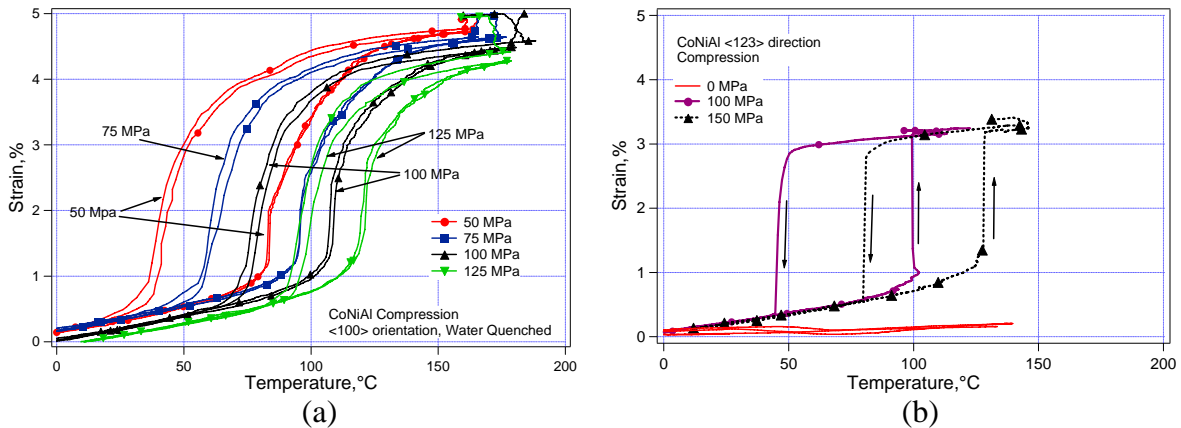


Figure 30. Compressive strain vs. temperature response of the a) [100] and b) [123] orientations under constant compressive stress.

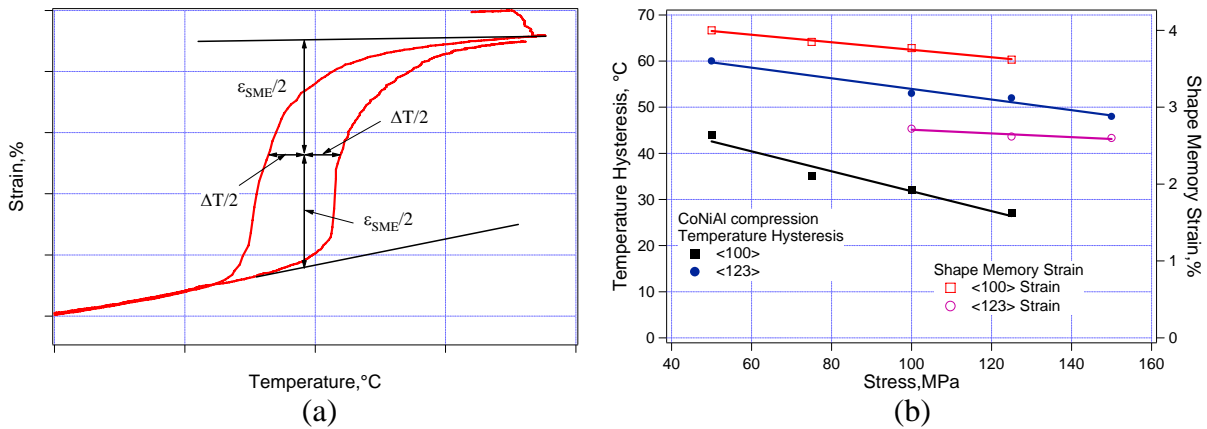


Figure 31: a) A schematic for the definitions of the temperature hysteresis (ΔT) and shape memory strain (ϵ_{SME}), b) Change in ΔT and ϵ_{SME} as a function of applied stress along different orientations.

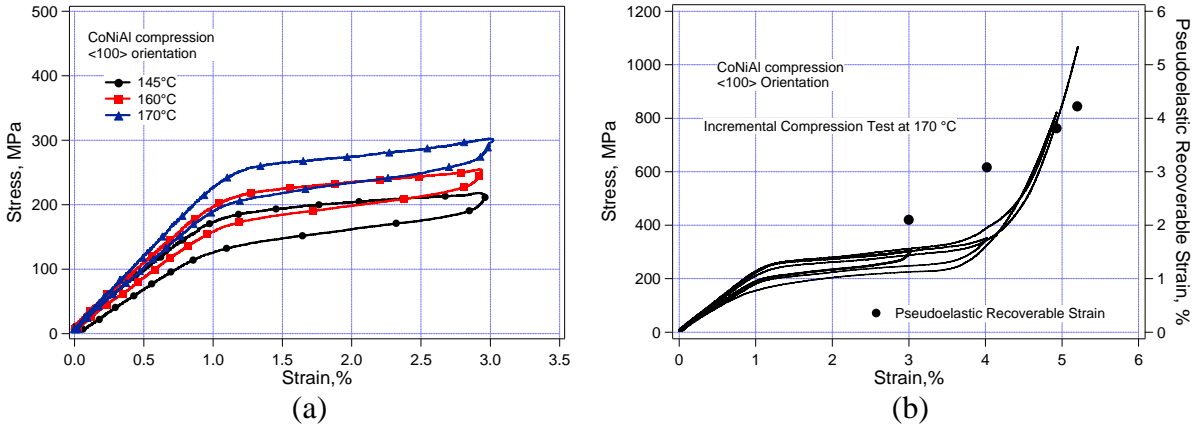


Figure 32. a) The temperature and b) strain dependence of the compressive pseudoelastic response of the [100] orientation.

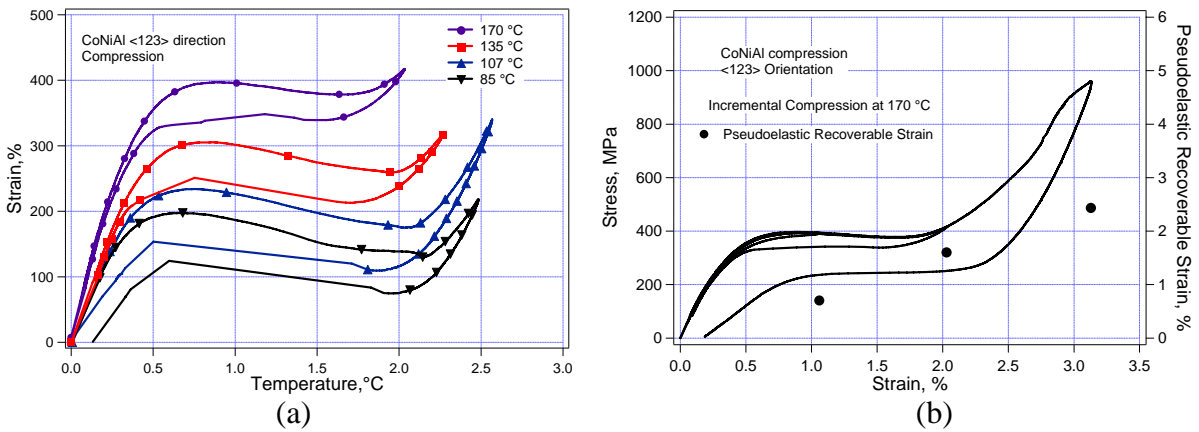


Figure 33: a) The temperature and b) the strain dependence of the compressive pseudoelastic response of the [123] orientation.

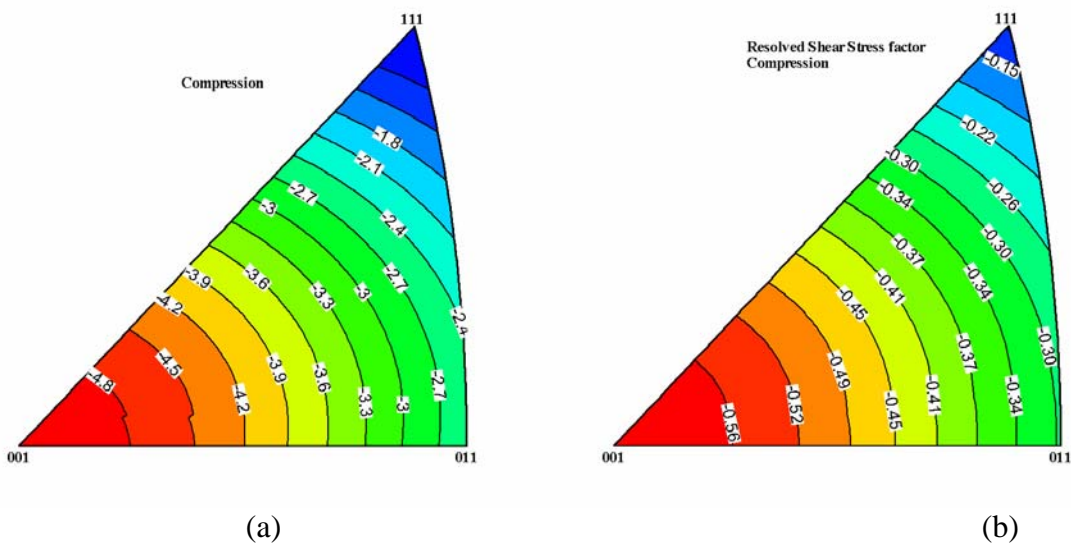


Figure 34. Transformation strain (a) and resolved shear stress factor (b) contours for the B2 to L₁₀ phase transformation in the present alloy under compression.

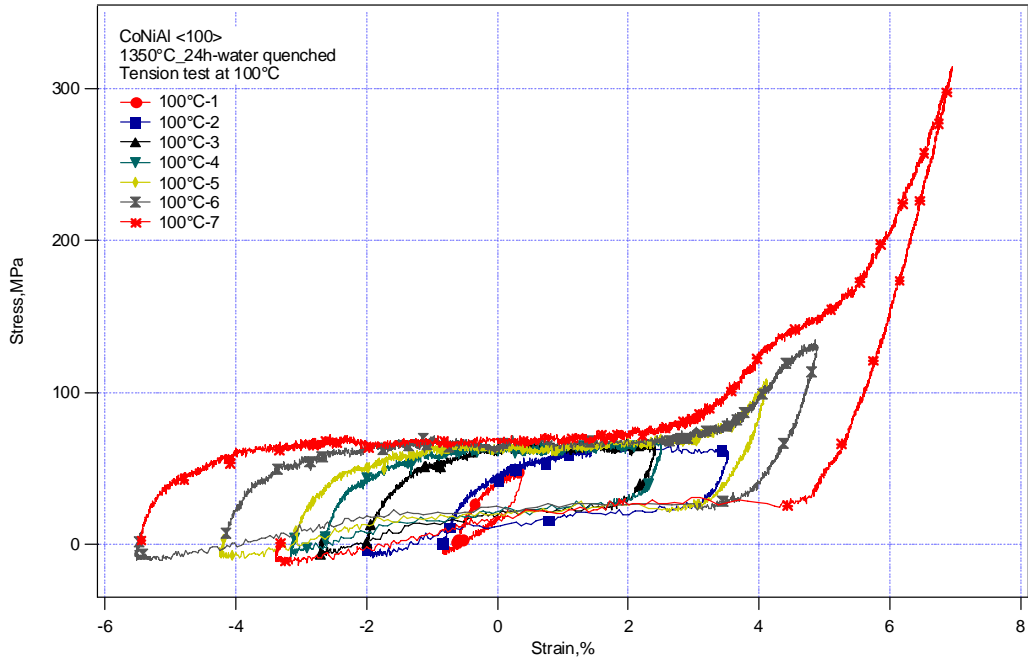
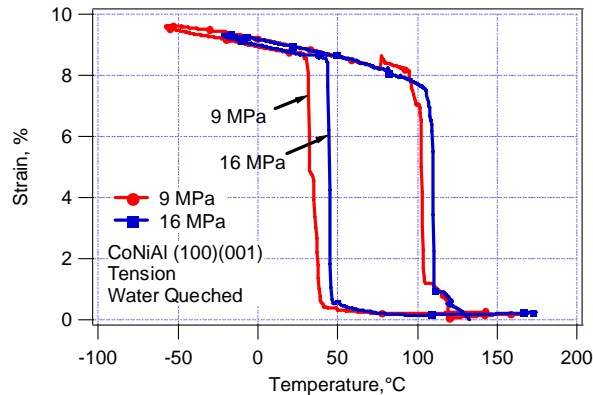
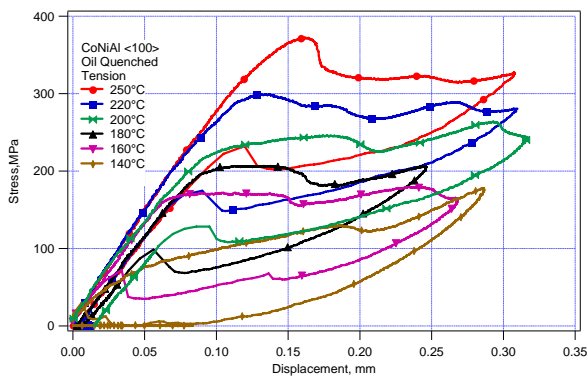


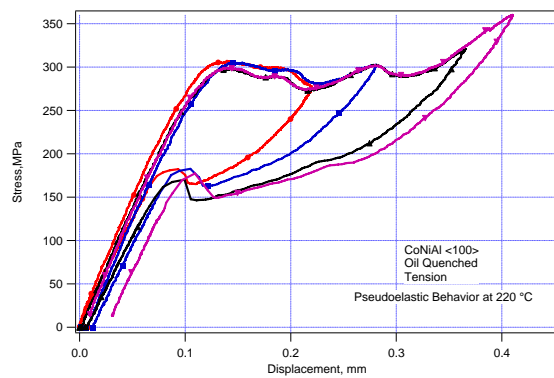
Figure 35. Tensile stress vs. strain response of the [100] single crystals of Co-33Ni-29Al (at%) at 100 °C showing the pseudoelastic response as a function of applied strain level.



(a)



(b)



(c)

Figure 36. Tension response of (a) the water-quenched [100] orientation of Co-33Ni-29Al (at%) during cooling-heating, (b) the oil quenched [110] orientation during pseudoelastic

straining at different temperatures showing the effect of temperature on the pseudoelastic stress level and stress hysteresis, and (c) the oil quenched [110] during pseudoelastic straining to different strain levels at 220 °C.

11. The detailed TEM investigations on the tension samples revealed interesting features. Figure 37 shows the microstructure of the [100] orientation after tension loading as shown in Figure 35. The $L1_0$ martensite phase is evident from the diffraction pattern with two variants of internal twins at room temperature. The internal twin plane is $[111]_{L1_0}$. Figure 38 shows the microstructure of the [123] orientation at room temperature after tensile deformation. The structure is B2 austenite as shown in the diffraction pattern since the M_s is below room temperature. The thin long features in this figure are not martensite plates but they are twins in the B2 phase. ***The interesting finding is that the twin plane is $[112]_{B2}$. Theoretically, it is impossible to form deformation twins with $[112]$ planes in B2 phase alloys [31]. B2 intermetallics are usually inherently brittle due to lack of available slip systems. Therefore, the activation of deformation twinning as an alternative deformation mechanism is desired since it provides additional ductility to B2 alloys.*** NiTi is a unique example of B2 alloys that experiences extensive deformation twinning and thus unusual ductility. Therefore, the observation of twins in a CoNiAl B2 alloy is a unique finding, however, the twinning plane of [112] is unusual. Recently, we have also observed this twinning mode after heavy deformation in NiTi [32] and we attributed it to the $B2 \rightarrow B19' \rightarrow B2$ transformation sequence as shown in Figure 39. Basically, the [112] twins originate from the compound twins in martensite. During the deformation of B2 phase, if the temperature is close to the transformation temperatures, stress induced martensitic transformation occurs and B19' is formed. Heavy deformation of B19' leads to formation of compound twins with high dislocation density especially accumulated along twin boundaries. Upon back transformation to B2, due to dislocation storage along the boundaries, internally twinned martensite does not transform back to single grain austenite, instead every twin in martensite transform into a twin in austenite. The exact lattice correspondence between these twins supports this hypothesis. Similarly, in CoNiAl, a similar mechanism should be responsible from the observation of high density of deformation twins in B2 CoNiAl after small deformation. Therefore, we argue that B2 first transform into $L1_0$ with internal twins and then these internal twins transform back to austenite as twins in austenite.

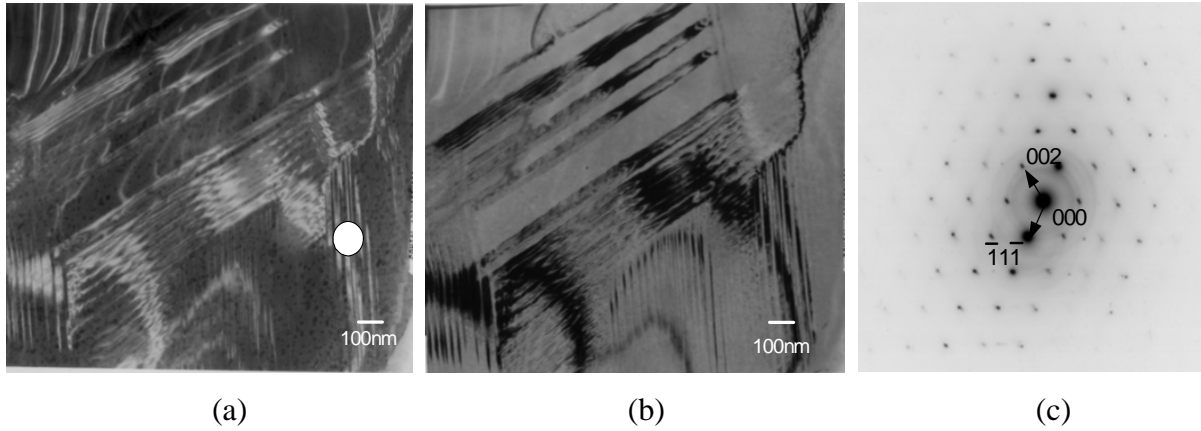


Figure 37. (a) Bright and (b) dark field TEM images of the [100] orientation of the Co-33Ni-29Al alloys after tensile deformation as shown in Figure 11. (c) shows that the structure is $L1_0$ martensite and the internal twin planes are (111) type.

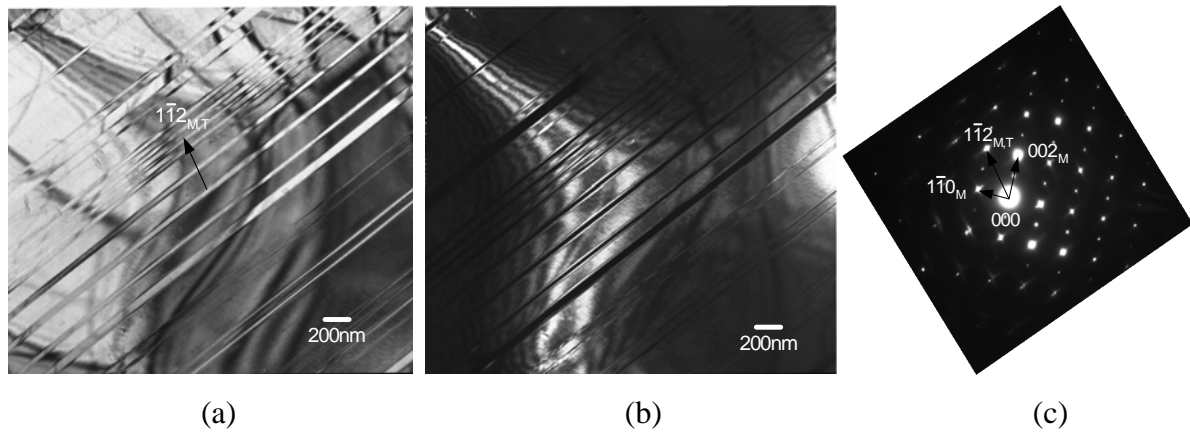


Figure 38. (a) Bright and (b) dark field TEM images of the [123] orientation of the Co-33Ni-29Al alloys after tensile deformation. (c) shows that the structure is B2 austenite and the features are deformation twins with the (112) type twinning plane.

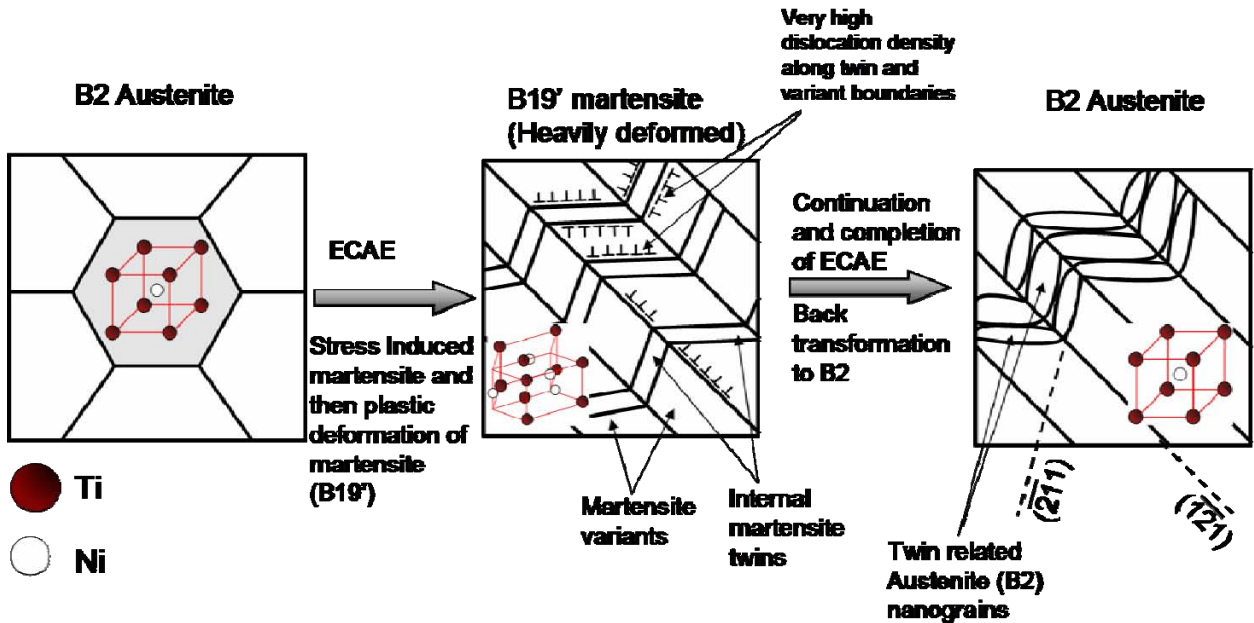


Figure 39. A schematic of the proposed mechanism of the deformation twin formation in B2 austenite during severe plastic deformation of 50.8 at.% NiTi via $B2 \xrightarrow{SIM} B19' \xrightarrow{SPD} B2$ transformation sequence. Please see the text for the details of the mechanism.

12. The pseudoelastic behavior of as-grown $Co_{49}Ni_{21}Ga_{30}$ single crystals oriented along the [001] direction was studied as a function of temperature. The compression axis along [001] was selected to curtail the dislocation activity in the parent phase as the austenitic slip system is $\{110\} \langle 001 \rangle$ in B2 crystals, which minimizes the influence of dislocation slip in the austenite on the formation of stress-induced martensite (SIM). The highest recoverable pseudoelastic strain with small stress hysteresis (< 30 MPa) reported here reaches 4.5 %. In addition, the single crystals studied demonstrated perfect pseudoelasticity at temperatures as high as 380 °C (Fig. 40). The alloys also exhibited an M_d temperature of about 425 °C with high strength levels (Fig. 41). At elevated temperatures 4 % pseudoelastic strain accompanied by large stress hysteresis of about 325 MPa was also achieved. *The above pseudoelastic characteristics makes CoNiGa alloys a promising ferromagnetic shape memory material for applications involving high temperature and high strength.*

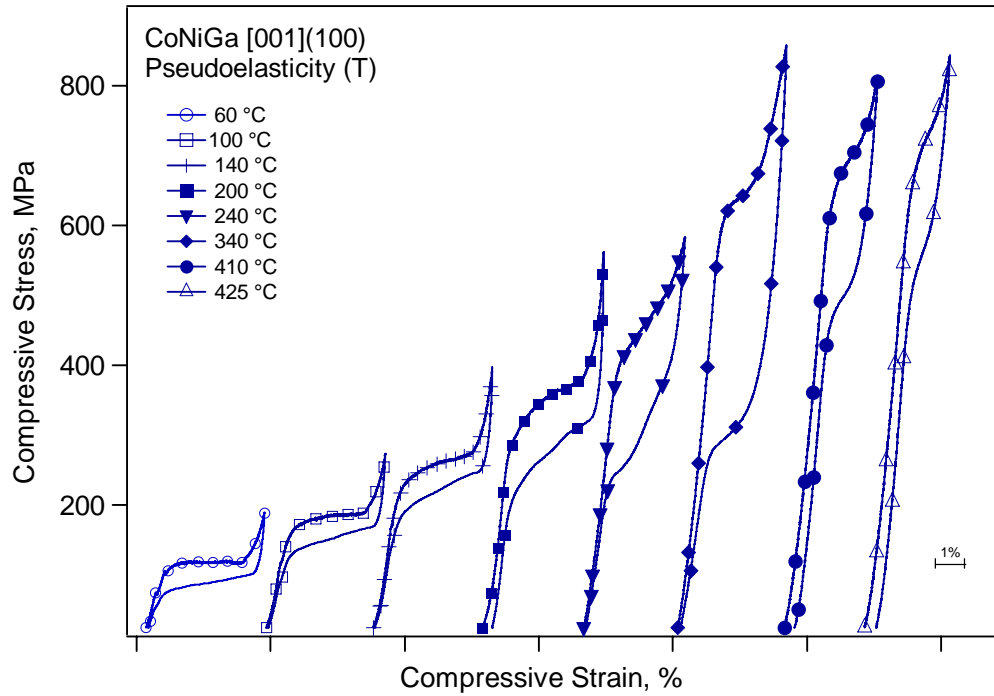


Figure 40: Pseudoelastic response of CoNiGa single crystals as a function of temperature.

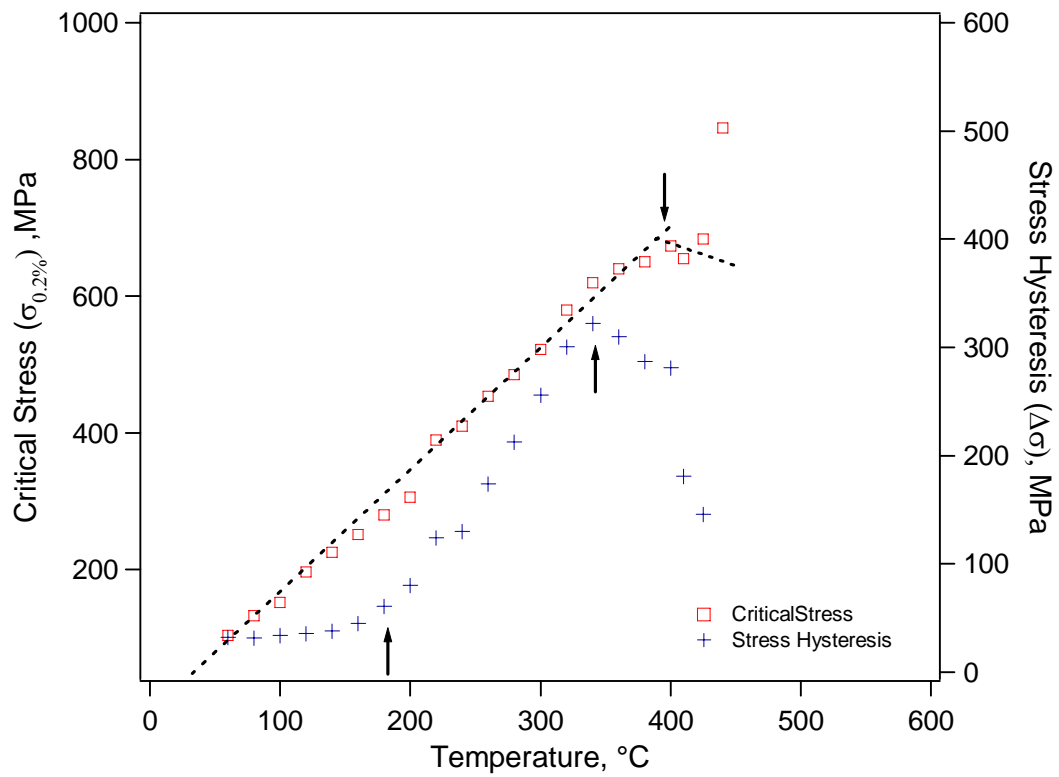


Figure 41: Critical stress and stress hysteresis vs temperature.

2.1. Modeling work

A phenomenological constitutive model for the magnetic field-induced shape memory effect in MSMA have been constructed [33]. The model describes the loading history dependent deformation as a function of the applied stresses and magnetic fields and captures the hysteretic effects in the material response by the means of internal state variables. From a literature review [21, 33-38] it had become evident, that the development of such a model was needed, since the constitutive response is dominated by dissipative effects associated with the strain hysteresis, but most existing models relied on energy minimization techniques in which dissipation can not be captured directly.

This model provided good predictability of the magnetic field-induced strain hysteresis curves [33, 39-40], but failed to give accurate predictions of the magnetization hysteresis. Several significant extensions have been made [39-41] to address this and other issues

1. The assumed constraint that the magnetization is fixed to the respective magnetic easy axes of the martensitic variants has been alleviated, with the introduction of additional internal state variables for the magnetization rotation. The magnetocrystalline anisotropy has therefore been acknowledged as being finite and it now appears explicitly in the free energy expression.
2. A different martensitic variant volume fraction has been introduced such that strain hysteresis loops, in which less than 100% of the second variant is produced, can be described more accurately.
3. With the new interpretation of the variant volume fraction and by identifying additional factors for the termination of the reorientation process, such as the full rotation of magnetization, it has become possible to predict the maximum reorientation strain produced in hysteresis loops under different bias stresses, and thus this information need no longer be provided as curve-fitted input data, as was previously the case.
4. Different and also newly developed hardening functions have been selected and tested to provide more accurate predictions of the material response with experiments.

In the following paragraphs, an outline of the model derivation will be given. The impact that the indicated extensions of the model have had on the applicability and accuracy of the model predictions will also be illustrated.

2.1.1. Derivation of the Model

The approach for modeling of the martensite variant reorientation process in magnetic shape memory alloys taken here is the following

- The constitutive model is phenomenological in nature and is based on a thermodynamically consistent framework.

- A free energy function is proposed for which the independent state variables that store energy in the system are identified.
- Dissipative effects are thermodynamically incorporated by introducing a set of internal variables.
- The model is rate independent. The onset and termination of the reorientation process can therefore be described by reorientation functions, i.e. associated critical values of the driving forces.
- Evolution equations are proposed for the internal variables based on the principle of maximum dissipation.

The construction of the total Gibbs free energy of the system is motivated by microstructure observed in MSMA martensite, which is schematically shown in Figure 42. The microstructural mechanisms by which the macroscopic shape and magnetization is modified are the variant twin boundary motion, magnetic domain wall motion and magnetization rotation. In the figure ξ denotes the variant 2 volume fraction, α the magnetic domain 2 volume fraction and θ_i the magnetization rotation angles. The free energy is proposed to be given by a weighted average of the contributions by each variant and magnetic domain. An additional mixing term accounts for the interaction between variants.

$$G = \hat{G}(T, \boldsymbol{\sigma}, \mathbf{H}, \xi, \boldsymbol{\varepsilon}^r, \alpha, \theta_i) = \xi \left[(1 - \alpha)G^2 + \alpha G^4 \right] + (1 - \xi) \left[(1 - \alpha)G^1 + \alpha G^3 \right] + G^{\text{mix}}$$

$$= -\frac{1}{2\rho} \boldsymbol{\sigma} : \mathbf{S}(\xi) \boldsymbol{\sigma} - \frac{\mu_0}{\rho} \mathbf{M}(\xi, \alpha, \theta_i) \cdot \mathbf{H} + G^{\text{an}}(\xi, \alpha, \theta_i) + \frac{1}{\rho} f^\xi(\xi, \boldsymbol{\varepsilon}^r) + \frac{1}{\rho} f^\alpha(\alpha) + G_0(T). \quad (2)$$

Therein T is the thermodynamic temperature, $\boldsymbol{\sigma}$ the Cauchy stress tensor and \mathbf{H} the magnetic field vector. The internal state variables are ξ , α , θ_i and additionally the reorientation strain tensor $\boldsymbol{\varepsilon}^r$. \mathbf{S} is the effective elastic compliance and \mathbf{M} is the effective magnetization. It has been assumed that the density does not differ in the two martensitic variants since the reorientation process is volume conserving.

By accounting for the nearly uniaxial symmetry of the magnetization of the tetragonal variants, the magnetocrystalline anisotropy term in the free energy expression is explicitly given by

$$G^{\text{an},i} = \sum_{n=0}^N K_n^i \sin^{2n}(\theta_i) = K_1 \sin^2(\theta_i), \quad (3)$$

where K_1 is a known anisotropy coefficient.

Without loss of generality, a special case is considered in which the magnetic domain volume fraction is fixed during the reorientation process. This assumption has often been in the literature and is supported by the observation that even for intermediate magnetic fields the domain distribution reduces to single domain configurations in each variant, which corresponds to a value of $\alpha = 0$ or 1, depending on the loading direction.

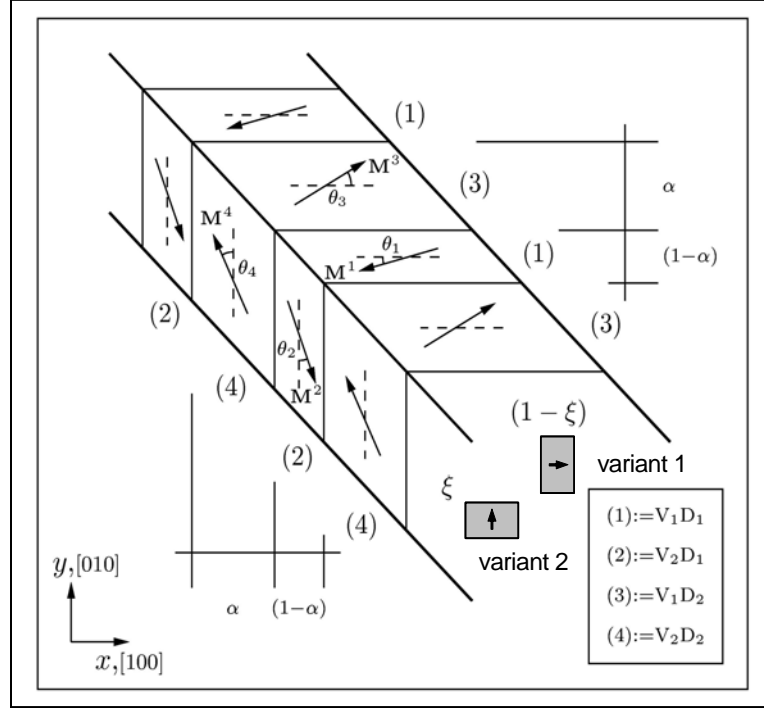


Figure 42: Schematic of martensitic variant and magnetic domain microstructure.

Constitutive relations for the dependent variables are obtained in terms of derivatives of the Gibbs free energy by following the well-known Coleman-Noll procedure which employs the Clausius-Duhem inequality (combination of the first and second law of thermodynamics)

$$-\left(\boldsymbol{\varepsilon}^e + \rho \frac{\partial \hat{G}}{\partial \boldsymbol{\sigma}}\right) : \dot{\boldsymbol{\sigma}} - \rho \left(s + \frac{\partial \hat{G}}{\partial T}\right) \dot{T} - \left(\mu_0 \mathbf{M} + \rho \frac{\partial \hat{G}}{\partial \mathbf{H}}\right) \cdot \dot{\mathbf{H}} + \left(\boldsymbol{\sigma} - \rho \frac{\partial \hat{G}}{\partial \boldsymbol{\varepsilon}^r}\right) : \dot{\boldsymbol{\varepsilon}}^r - \rho \frac{\partial \hat{G}}{\partial \bar{\boldsymbol{\zeta}}} \cdot \dot{\bar{\boldsymbol{\zeta}}} \geq 0, \quad (4)$$

with $\bar{\boldsymbol{\zeta}} = (\xi, \alpha, \theta_i)$ representing the list of internal state variables. The thermoelastic strain and the magnetization for example are then given by

$$\boldsymbol{\varepsilon}^{te} = -\rho \frac{\partial \hat{G}}{\partial \boldsymbol{\sigma}} = \mathbf{S} \boldsymbol{\sigma},$$

$$\mathbf{M} = -\frac{\rho}{\mu_0} \frac{\partial \hat{G}}{\partial \mathbf{H}} = M_s (1 - \xi) [\cos(\theta_3) \mathbf{e}_x + \sin(\theta_3) \mathbf{e}_y] + M_s \xi [-\sin(\theta_4) \mathbf{e}_x + \cos(\theta_4) \mathbf{e}_y], \quad (5)$$

where M_s is the saturation magnetization.

The expression for the evolution of the reorientation strain based on the principle of maximum dissipation is given by

$$\dot{\boldsymbol{\varepsilon}}^r = \boldsymbol{\Lambda}^r \dot{\bar{\boldsymbol{\zeta}}} \quad (6)$$

where $\boldsymbol{\Lambda}^r$ is the reorientation strain tensor.

We can then define a thermodynamic driving force for the reorientation process that is conjugate to the variant volume fraction ξ ,

$$\pi^\xi := \boldsymbol{\sigma}^{\text{eff}} : \boldsymbol{\Lambda} - \rho \frac{\partial G}{\partial \xi}, \quad \boldsymbol{\sigma}^{\text{eff}} := \boldsymbol{\sigma} - \rho \frac{\partial G}{\partial \boldsymbol{\varepsilon}^r}. \quad (7)$$

The Clausius-Duhem inequality then reduces to $\pi^\xi \dot{\xi} \geq 0$. With the assumed rate independence it is thus possible to postulate the following reorientation conditions

$$\begin{aligned} \dot{\xi} \geq 0, \quad \pi^\xi \leq Y^\xi, \quad \dot{\xi} \cdot [\pi^\xi - Y^\xi] &= 0 \\ \dot{\xi} \leq 0, \quad \pi^\xi \geq -Y^\xi, \quad \dot{\xi} \cdot [-\pi^\xi - Y^\xi] &= 0, \end{aligned} \quad (8)$$

where Y^ξ is the critical value for the driving force. An additional assumption that the magnetization rotation is represents a reversible process leads to additional constraints with the help of which one can eliminate the explicit dependence on the θ_i .

The hardening behavior during reorientation is approximated by the following polynomial hardening function

$$\rho G^{\xi\text{-mix}}(\xi, \boldsymbol{\varepsilon}^r) = f^\xi(\xi, \boldsymbol{\varepsilon}^r) = \begin{cases} \frac{1}{2} A \xi^2 + (B_1 + B_2) \xi, & \xi > 0 \\ \frac{1}{2} C \xi^2 + (B_1 - B_2) \xi, & \xi < 0 \end{cases} \quad (9)$$

2.1.2. A numerical example of the application of the model

For a special loading case, which is schematically depicted in Figure 43, the following simplifications apply

$$\boldsymbol{\sigma} = \begin{bmatrix} \sigma & 0 & 0 \\ 0 & 0 & 0 \\ 0 & 0 & 0 \end{bmatrix}, \quad \sigma < 0, \quad \mathbf{H} = \begin{pmatrix} 0 \\ H_y \\ 0 \end{pmatrix}, \quad H_y > 0, \quad \boldsymbol{\sigma}^{\text{eff}} : \boldsymbol{\Lambda} = \sigma \boldsymbol{\varepsilon}^{\text{max}}. \quad (10)$$

The evolution of the martensitic volume fraction for the forward reorientation process ($\pi^\xi = Y^\xi$) is given by

$$\xi^{1 \rightarrow 2} = \frac{1}{A} \left[\sigma \boldsymbol{\varepsilon}^{\text{max}} + \mu_0 M_s H_y - \frac{(\mu_0 M_s)^2}{4 \rho K_1} H_y^2 - B_1 - B_2 - Y^\xi \right], \quad (11)$$

whereas the reverse process ($\pi^\xi = -Y^\xi$) is characterized by

$$\xi^{2 \rightarrow 1} = \frac{1}{C} \left[\sigma \varepsilon^{\max} + \mu_0 M_s H_y - \frac{(\mu_0 M_s)^2}{4 \rho K_1} H_y^2 - B_1 + B_2 + Y^\xi \right]. \quad (12)$$

The hardening parameters introduced in the model can be related to the measurable magnetic field values at which the reorientation start and finish lines are intersected in the following manner (cf. Figure 44).

$$\begin{aligned} A &= \mu_0 M_s (H_f^{1,2} - H_s^{1,2}) - \frac{(\mu_0 M_s)^2}{4 \rho K_1} \left[(H_f^{1,2})^2 - (H_s^{1,2})^2 \right] \\ B_1 &= \frac{1}{2} \mu_0 M_s (H_s^{1,2} + H_f^{2,1}) - \frac{(\mu_0 M_s)^2}{8 \rho K_1} \left[(H_s^{1,2})^2 + (H_f^{2,1})^2 \right] + \sigma^* \varepsilon^{\max} \\ B_2 &= \frac{1}{4} (C - A) \\ C &= \mu_0 M_s (H_s^{2,1} - H_f^{2,1}) - \frac{(\mu_0 M_s)^2}{4 \rho K_1} \left[(H_s^{2,1})^2 - (H_f^{2,1})^2 \right] \\ Y^\xi &= \frac{1}{2} \mu_0 M_s (H_s^{1,2} - H_f^{2,1}) - B_2 \end{aligned} \quad (13)$$

Note that beyond material constants such as the density, the saturation magnetization and the anisotropy constant, only a single experimental loop at an arbitrary level of the constant biasing stress σ^* is sufficient to determine these model parameters. The remaining constant that is needed as input to the model is the maximum strain value for full reorientation, which can be taken from the measured hysteresis loop or estimated from the lattice parameters of the considered martensite.

The following set of parameters was obtained from data presented in the literature [42], -1 Mpa.

$$\begin{aligned} \rho &= 8000.0 \text{ kgm}^{-3}, & \mu_0 H_s^{1,2} &= 0.35 \text{ T}, \\ \rho K_1 &= 1.67 \cdot 10^5 \text{ Jm}^{-3}, & \mu_0 H_f^{1,2} &= 0.6 \text{ T}, \\ M_s &= 0.514 \cdot 10^6 \text{ Am}^{-1}, & \mu_0 H_s^{2,1} &= 0.32 \text{ T}, \\ \varepsilon^{\max} &= 0.062, & \mu_0 H_f^{2,1} &= -0.08 \text{ T}. \end{aligned} \quad (14)$$

An interesting visualization of the reorientation condition (8), based on these data, is provided by the phase diagram in stress vs. magnetic field space which is plotted in Figure 44.

Figure 45 shows the simulation of the magnetic field-induced strain loop under -1.0 Mpa. and the prediction of the loops for -1.2 Mpa and -1.4 Mpa, respectively. It is observed that all of the important features of the constitutive behavior are captured by the model prediction,

namely the hysteretic nature and the stress dependence of the hysteresis size and shape. Note also the prediction of the so-called first cycle effect, which leads to unsymmetric hysteresis loops under positive and negative applied magnetic fields.

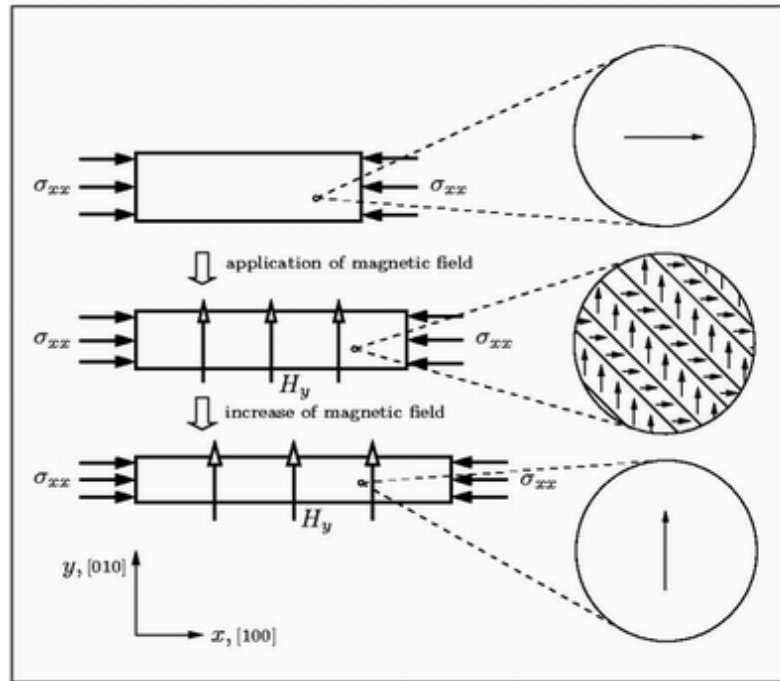


Figure 43: Phase diagram for the variant reorientation process in MSMA.

Figure 46 depicts the corresponding magnetization curves. It is evident from the later that the additional mechanism of magnetization rotation significantly changes the character of the magnetization hysteresis and that the extended model leads to much improved predictions of these curves.

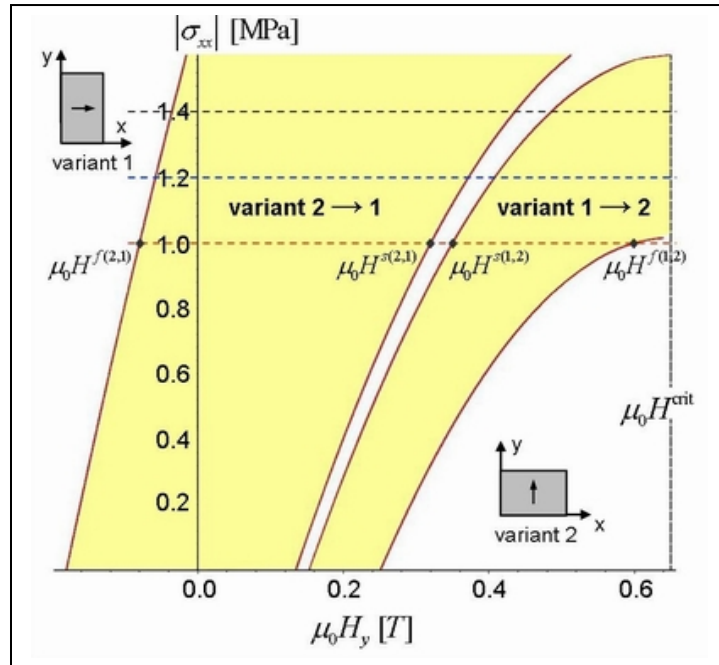


Figure 44: Phase diagram for the variant reorientation process in MSMA.

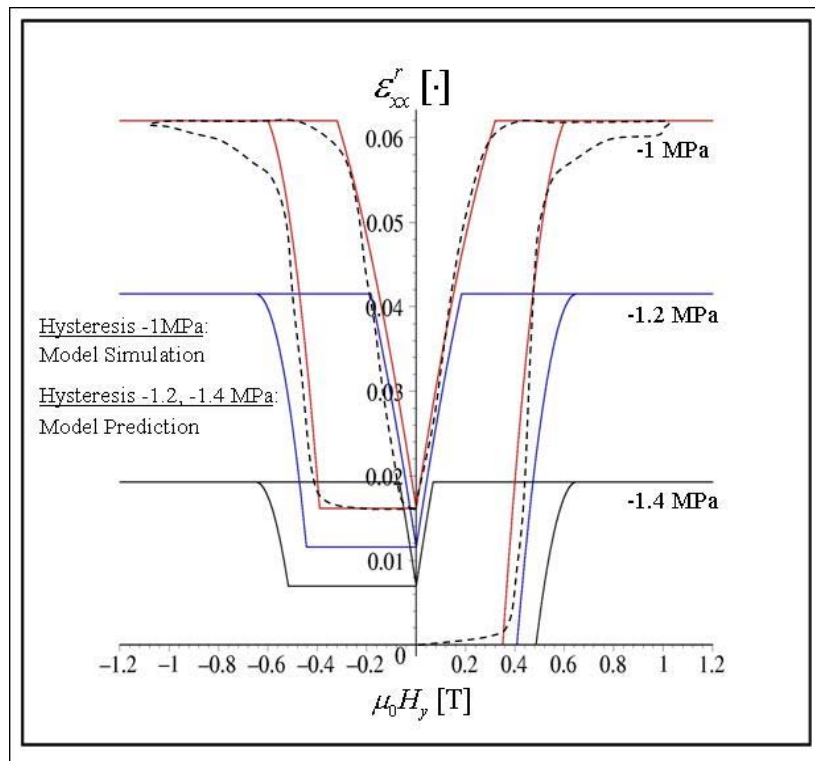


Figure 45: Model prediction of magnetic field-induced strain hysteresis. Numerical results (solid lines), experimental data published in Heczko et al. 2003 (dashed line) [42].

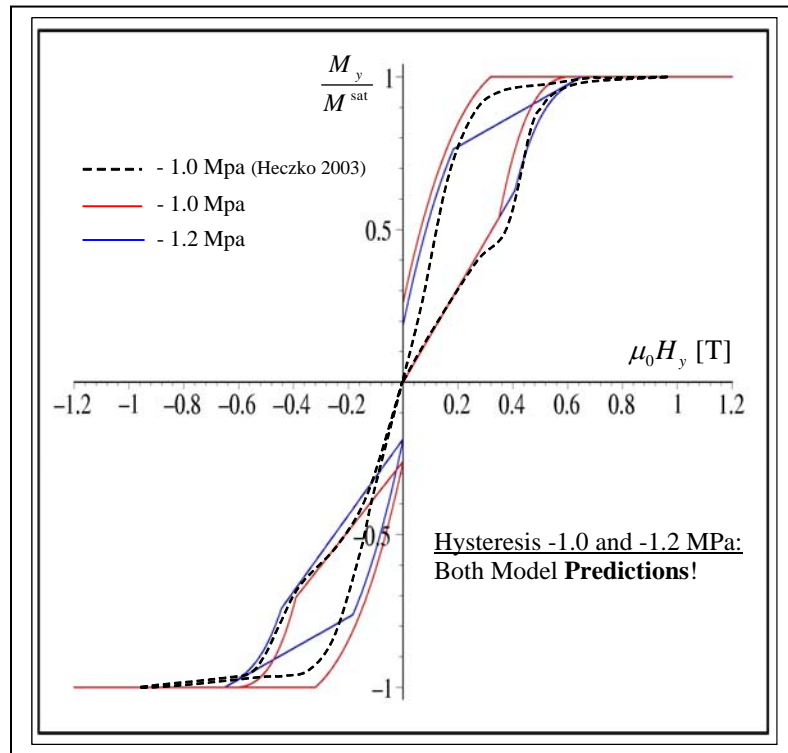


Figure 46: Model prediction of magnetic field-induced magnetization hysteresis. Numerical results (solid lines), experimental data published in Heczko et al. 2003 (dashed line) [42].

3. Listing of all publications and technical reports supported under this grant or contract

(a) *Papers published in peer reviewed journals*

1. H.E. Karaca, I. Karaman, B. Basaran, Y.I. Chumlyakov, and H.J. Maier, 2006, "Magnetic Field and Stress Induced Martensite Reorientation in NiMnGa Ferromagnetic Shape Memory Alloy Single Crystals," *Acta Materialia*, Vol. 54, pp. 233-245.
2. D. Meyer, H.J. Maier, J. Dadda, I. Karaman, and H.E. Karaca, 2006, "Thermally and Stress-Induced Martensitic Transformation in CoNiAl Ferromagnetic Shape Memory Alloy Single Crystals," *Materials Science and Engineering A*, in press.
3. B. Kiefer and D.C. Lagoudas, 2005, "Magnetic Field-Induced Martensitic Variant Reorientation in Magnetic Shape Memory Alloys," *Philosophical Magazine*, Vol. 85, pp. 4289-4329.
4. H.E. Karaca, I. Karaman, Y.I. Chumlyakov, D.C. Lagoudas, and X.Y. Zhang, 2004, "Compressive Response of A Single Crystalline CoNiAl Shape Memory Alloy," *Scripta Materialia*, Vol. 51, pp. 261-266.
5. Y.I. Chumlyakov, I.V. Kireeva, I. Karaman, E.Yu. Panchenko, E.G. Zakharova, A.V. Tverskov, A.V. Ovsyannikov, K.M. Nazarov, and V.A. Kirillov, 2004, "Orientational Dependence of Shape Memory Effects and Superelasticity in CoNiGa, NiMnGa, CoNiAl, FeNiCoTi, and TiNi Single Crystals," *Russian Physics Journal*, Vol. 47, No.9, pp. 893-911.
6. H.E. Karaca, I. Karaman, D.C. Lagoudas, H.J. Maier, and Y.I. Chumlyakov, 2003, "Recoverable Stress Induced Martensitic Transformation in a Ferromagnetic CoNiAl Alloy," *Scripta Materialia*, Vol. 49, pp. 831-838.

(b) *Papers published in non-peer-reviewed journals or in conference proceedings*

1. B. Kiefer and D.C. Lagoudas, "Modeling of the Magnetic Field-Induced Martensitic Variant Reorientation and the Associated Magnetic Shape Memory Effect in MSMAs", *Proceedings of SPIE, Smart Structures and Materials: Active Materials: Behavior and Mechanics*, San Diego, CA, 6–10 March 2005, Vol. 5761, 2005, pp. 454–465.
2. B. Kiefer and D.C. Lagoudas, "Phenomenological Modeling of Ferromagnetic Shape Memory Alloys," *Proceedings of SPIE, Smart Structures and Materials: Active Materials: Behavior and Mechanics*, San Diego, CA, 14-18 March 2004, Vol. 5387, pp. 164-176.

(c) *Papers presented at meetings, but not published in conference proceedings*

1. I. Karaman, H.E. Karaca, D.C. Lagoudas and H.J. Maier, "Magnetic Field Induced Martensite Reorientation and Martensite to Austenite Phase Transformation in NiMnGa and CoNiAl Single Crystals: Guidelines to Increase The Blocking Stress," *Workshop on Magnetic Shape Memory Alloys*, September 11-16, 2005, Ascona, Switzerland, 2005.
2. I. Karaman, H.E. Karaca, B. Basaran, Y.I. Chumlyakov, and H.J. Maier, "Magnetic and Conventional Shape Memory Characteristics of $\text{Co}_{38}\text{Ni}_{33}\text{Al}_{29}$ and Ni_2MnGa Shape Memory Alloys," *The International Conference on Martensitic Transformations (ICOMAT 05)*, June 14-17, 2005, Shanghai, China, 2005.

3. D.C. Lagoudas, I. Karaman, I., and B. Kiefer, "Experimental Investigation and Constitutive Modeling of the Magnetic Shape Memory Effect Caused by Martensitic Variant Rearrangement," Symposium on "Coupled Nonlinear Phenomena, Modeling and Simulation for Smart, Ferroic, and Multiferroic Materials", MRS Spring 2005 Meeting, March 28 – April 1, 2005, San Francisco, CA, 2005.
4. H.E. Karaca, B. Basaran, I. Karaman, Y.I. Chumlyakov, and H.J. Maier, "Magnetic and Conventional Shape Memory Characteristics of $\text{Co}_{38}\text{Ni}_{33}\text{Al}_{29}$ and Ni_2MnGa Shape Memory Alloys," Conference on Active Materials: Behavior and Mechanics, The International Society for Optical Engineering (SPIE) 12th Annual International Symposium on Smart Structures and Materials, March 6-10, 2005, San Diego, CA, 2005.
5. B. Kiefer and D.C. Lagoudas, "Modeling of the Magnetic Field-Induced Martensitic Variant Reorientation and the Associated Magnetic Shape Memory Effect in MSMAs," 2005 SPIE/ASME Best Student Paper Presentation Contest, 12th SPIE International Symposium: Smart Structures and Materials, San Diego, CA, 6-10 March 2005.
6. D.C. Lagoudas and B. Kiefer, "Constitutive Modeling of the Ferromagnetic Shape Memory Effect under Special Consideration of the Evolution of Magnetic Domains," ASME International Mechanical Engineering Congress: Aerospace: Adaptive Materials and Systems: Shape Memory Alloys I, Anaheim, CA, 13-19 November 2004.
7. D.C. Lagoudas, I. Karaman, I., and B. Kiefer, "Investigation of the Influence of the Magnetic Microstructure on the Martensitic Variant Reorientation Process in Magnetic Shape Memory Alloys," Symposium on Active Materials and Structures, held at 41th Annual Technical Meeting of the Society of Engineering Sciences, October 10-13, 2004, Lincoln, NE, 2004.
8. H.E. Karaca, I. Karaman, J.S. Mather, B.W. Bagley, and Y.I. Chumlyakov, "Fundamental Shape Memory Characteristics of New CoNiAl Shape Memory Alloys," Conference on Active Materials: Behavior and Mechanics, The International Society for Optical Engineering (SPIE) 11th Annual International Symposium on Smart Structures and Materials, March 14-18, 2004, San Diego, CA, 2004.
9. H.E. Karaca, I. Karaman, and Y.I. Chumlyakov, "Thermally and Stress Induced Martensitic Transformation in New CoNiAl Shape Memory Alloys," TMS 2004 Annual Meeting, March 14-18, 2004, Charlotte, NC, 2004.
10. I. Karaman, H.E. Karaca, and D.C. Lagoudas, "Thermally and Stress Induced Martensitic Transformation in New CoNiAl Shape Memory Alloys," 2003 ASME – IMECE International Mechanical Engineering Congress and RD&D Expo, November 15-21, 2003, Washington, D.C., 2003.
11. D.C. Lagoudas, I. Karaman, B. Kiefer, and P. Entchev, "A Phenomenological Model for Magnetic Shape Memory Alloys with Hysteresis Effects," 2003 ASME – IMECE International Mechanical Engineering Congress and RD&D Expo, November 15-21, 2003, Washington, D.C., 2003.
12. D.C. Lagoudas, I. Karaman, B. Kiefer, P. Entchev, and H.E. Karaca, "A Phenomenological Model Based on the Experimental Characterization of Ferromagnetic Shape Memory Alloy Systems," Symposium on Shape Memory

- Materials, held at 40th Annual Technical Meeting of Society of Engineering Sciences, October 12-15, 2003, Ann Arbor, MI, 2003.
13. H.E. Karaca and I. Karaman, "Thermally and Stress Induced Martensitic Transformation in New CoNiAl Shape Memory Alloys," 2003 ASME Mechanics and Materials Conference, June 17-20, 2003, Scottsdale, AZ, 2003.

(d) *Manuscripts submitted but not published*

1. I. Karaman, H.E. Karaca, B. Basaran, D.C. Lagoudas, Y.I. Chumlyakov, and H.J. Maier, 2006, "Reversible Magnetic Field-Induced Phase Transformation for High Actuation Stress and Work Output," submitted to Science, 2006.
2. I. Karaman, H.E. Karaca, B. Basaran, D.C. Lagoudas, Y.I. Chumlyakov, and H.J. Maier, 2006, "Magnetic Field Induced Phase Transformation in NiMnGa Ferromagnetic Shape Memory Alloy Single Crystals," submitted to Acta Materialia, 2006.
3. B. Kockar, I. Karaman, and Y.I. Chumlyakov, 2006, "The Effect of Aging on Martensitic Transformation of a CoNiAl Ferromagnetic Shape Memory Alloy," submitted to Materials Science and Engineering A, 2006.
4. B. Kiefer, H.E. Karaca, D.C. Lagoudas, and I. Karaman, 2005, "Experimental Investigation and Constitutive Modeling of the Field-Induced Variant Rearrangement in Ni₂MnGa Magnetic Shape Memory Alloys," submitted to Journal of Magnetism and Magnetic Materials, 2005.

(e) *Technical reports submitted to ARO*

Three interim progress reports.

4. List of all Participating Scientific Personnel showing any Advanced Degrees Earned by them while employed on the Project

- a) Dr. I. Karaman (PI): Texas A&M University - Material characterization and mechanical properties
- b) Dr. D.C. Lagoudas (Co-PI): Texas A&M University – Modeling
- c) Robert Barber (Research Associate/Engineer): Texas A&M University – Die/tool/fixture design and materials processing
- d) Bjoern Kiefer (Graduate Research Assistant - Ph.D. Student): Texas A&M University – Modeling
- e) Haluk Ersin Karaca (Graduate Research Assistant – Ph.D. Student): Texas A&M University – Microstructural characterization and magnetothermomechanical property characterization. He earned his M.S. degree working in this project.
- f) Burak Basaran (Graduate Research Assistant – Ph.D. Student): Texas A&M University – Magnetothermomechanical test set-up design, building and property characterization.
- g) Benat Kockar (Graduate Research Assistant – Ph.D. Student): Texas A&M University – Microstructural characterization.
- h) Joseph S. Mather (Undergraduate Research Assistant): Texas A&M University – Magnetothermomechanical test set-up design and building, cooling-heating set-up

design and building. He earned his B.S. degree working in this project. He is currently a Ph.D. student at UIUC.

- i) Kathryn Sy (Undergraduate Research Assistant): Texas A&M University – Physical and microstructural characterizations. She earned her B.S. degree working in this project. She is currently an M.S. student at TAMU.

5. Report of Inventions

None

6. Bibliography

1. I. Takeuchi *et al.*, *Nature Mater.* **2**, 180 (2003).
2. K. Ullakko, J.K. Huang, C. Kantner, R.C. O’Handley, V.V. Kokorin, *Appl. Phys. Lett.* **69**, 1966 (1996).
3. S.J. Murray *et al.*, *J. Appl. Phys.* **87**, 5774 (2000).
4. A. Sozinov, A.A. Likhachev, N. Lanska, K. Ullakko, *Appl. Phys. Lett.* **80**, 1746 (2002).
5. M.A. Marioni *et al.*, *J. Magn. Magn. Mater.* **290-291**, 35 (2005).
6. H.E. Karaca, I. Karaman, B. Basaran, Y.I. Chumlyakov, H.J. Maier, *Acta Mater.* **54**, 233 (2006).
7. R.C. O’Handley, *J. Appl. Phys.* **83**, 3263 (1998).
8. I. Suorsa, E. Pagounis, K. Ullakko, *J. Magn. Magn. Mater.* **272-276**, 2029 (2004).
9. O. Heczko, A. Sozinov, K. Ullakko, *IEEE Trans. on Magn.* **36**, 3266 (2000).
10. R.D. James, R. Tickle, M. Wuttig, *Mater Sci Eng A* **273-275**, 320 (1999).
11. C.P. Sasso, M. Pasquale, G. Bertotti, V.A. L’vov, V.A. Chernenko, *IEEE Trans. Magn.* **39**, 3399 (2003).
12. O. Heczko, L. Straka, *J. Appl. Phys.* **94**, 7139 (2003).
13. S.J. Murray *et al.*, *J. Appl. Phys.* **83**, 7297 (1998).
14. M.J. Dapino, *Struct. Eng. Mech.* **17**, 303 (2004).
15. J.Y. Li, R.C. Rogan, E. Üstündag, K. Bhattacharya, *Nature Mater.* **4**, 776 (2005).
16. M. Wun-Fogle, J.B. Restorff, K. Leung, J.R. Cullen, A.E. Clark, *IEEE Trans. Magnetics* **35**, 3817 (1999).
17. J. Fan, W.A. Stoll, C.S. Lynch, *Acta Mater.* **47**, 4415 (1999).
18. K. Otsuka, C.M. Wayman, *Shape memory materials* (Cambridge University Press, New York, NY, 1998).

19. C.P. Henry, D. Bono, J. Feuchtwanger, S.M. Allen, R.C. O'Handley, *J. Appl. Phys.* **91**, 7810 (2002).
20. T. Yamamoto *et al.*, *Acta Mater.* **52**, 5083 (2004).
21. R.D. James, M. Wuttig, *Phil. Mag. A* **77**, 1273 (1998).
22. T. Kakeshita *et al.*, *Mater. Trans. JIM* **41**, 882 (2000).
23. X.J. Hao, H. Ohtsuka, *Mater. Sci. Forum* **475-479**, 301 (2005).
24. T. Kakeshita, K. Shimizu, S. Funada, M. Date, *Acta Metal.* **33**, 1381 (1985).
25. K.R. Satyanar, W. Eliaz, A.P. Miodowni, *Acta Metall.* **16**, 877 (1968).
26. V. M. Segal, *Mat. Sci. Eng. A.*, **A197**, 157 (1995).
27. L.R. Cornwell, K.T. Hartwig, R.E. Goforth and S.L. Semiatin, *Mat. Char.*, **37**, 295 (1996).
28. W. M. Segal, V.I. Reznikov, A.E. Drbyshevskiy and V.L. Kopylov, *Rus. Metall. Engl. Trans.*, **1**, 115 (1981).
29. K.T. Hartwig, H. Zapata, A. Parasiris and S.N. Mathaudhu, in *Powder Materials: Current Research and Practices*, edited by F.D.S. Marquis, N.N. Thadhani and E.V. Barrera (TMS Publishing, Warrendale, PA, 2001) p. 211.
30. <http://ndea.jpl.nasa.gov/nasa-nde/lommas/eap/actuators-comp.pdf>
31. W.J. Moberly, J.L. Proft, T.W. Duerig, R. Sinclair, R., 1990, *Acta Metall. Mater.*, **38**, 1601.
32. I. Karaman, A. V. Kulkarni, and Z.P. Luo, 2005, *Philosophical Magazine*, Vol. 85, pp. 1729-1745.
33. Lagoudas, D.C. and Kiefer, B., *Proceedings of SPIE, 11th Annual International Symposium: Smart Structures and Materials*, San Diego CA, 14-18 March, 2004, Vol. 5387, 164-176.
34. R.D. James and K.F. Hane, *Acta Mater*, 2000, Vol. 48, 197.
35. Tickle, R. and James, R. D., *Journal of Magnetism and Magnetic Materials*, 1999, Vol. 195, pp. 627-638.
36. Tickle, R., 2000, *Ferromagnetic Shape Memory Materials*, Dissertation, University of Minnesota.
37. O'Handley, R.C., *Journal of Applied Physics*, 1998, Vol 83 (6), pp. 3263-3270.
38. Likhachev, A. A. and Ullakko, K., *The European Physical Journal B*, 2000, Vol. 14, pp. 263-267.
39. Kiefer, B., Lagoudas, D.C., Karaman, I., and Karaca, H.E., Submitted to *Journal of Magnetism and Magnetic Materials*, 2005.

40. B. Kiefer and D.C. Lagoudas, 2005, “Magnetic Field-Induced Martensitic Variant Reorientation in Magnetic Shape Memory Alloys,” *Philosophical Magazine*, Vol. 85, pp. 4289-4329.
41. B. Kiefer and D.C. Lagoudas, “Modeling of the Magnetic Field-Induced Martensitic Variant Reorientation and the Associated Magnetic Shape Memory Effect in MSMAs”, *Proceedings of SPIE, Smart Structures and Materials: Active Materials: Behavior and Mechanics*, San Diego, CA, 6–10 March 2005, Vol. 5761, 2005, pp. 454–465.
42. Heczko, O., Straka, L. and Ullakko, K., *Journal de Physique IV*, 2003, Vol. 112, pp. 959-962.

7. Appendices

None